4. DOCUMENTATION AND ANALYSIS OF FRACTURES IN THE LARGE BLOCK TEST

Fractures were carefully mapped on the block surface, and information on fracturing was also collected from cores and video logs of boreholes (Wagoner 1999; Wagoner 2000). The fractures were evaluated for their significance on the basis of size, extent, and other considerations, and the major fractures were selected to be included in a 3-D model. Although the LBT is not being used to characterize YM, its usefulness as a test of processes, models, and so forth is enhanced if the rock mass is similar to the repository horizon rock mass. For this reason, Fran Ridge was selected. Although the stress conditions are not the same and fracture apertures thus will not necessarily be the same, it is helpful if the fractures are similar in distribution to those in the repository. Therefore, the second analysis was of the fracture distribution compared with that of the main Exploratory Studies Facility (ESF) drift that is in the repository horizon. The fractures in the LBT were dominated by high-angle fractures. This is similar to the fractures in the ESF of Yucca Mountain. However, the fracture orientation in the block is somewhat different from that in the ESF (Section 2.2.1, Wilder et al. 1997).

Characterization of the block began with mapping and analysis of the distribution of fractures. Fractures were carefully mapped using a 1 ft × 1 ft grid system on all four vertical sides and the top of the block (see Figure 4-1). Fracture mapping started September 19, 1994, and was completed October 6, 1994. Each fracture was assigned a unique number on each side of the block, and fracture attitudes were measured where possible. Fracture surface roughness was not recorded. More than 2400 individual fractures were mapped. The range and distribution of fracture lengths are recorded in Table 4-1. The fracture locations were digitized, and fracture segment nodes were assigned x-y-z values. These scattered data points were then input into a 3-D modeling code (EarthVision™ version 5.0). The resulting surface fracture distribution is shown in Figure 4-1; Table 4-1 lists fractures ordered by length and shows that most of the fractures are less than 1 m long.

Numerous boreholes were drilled in the large block for installation of monitoring instrumentation and observation. Figure 4-2 shows the location of those boreholes. The angled boreholes (color-coded yellow) are the post-test boreholes.

Fracture data were also collected from the borehole video logs of these holes. Information on the core is not included in this document. Detailed fracture information from the video logs is available in Appendix C. Seventy-one boreholes were videotaped. In that process, a measuring tape was placed in the borehole for location purposes. In the case of the vertical boreholes, the tape was hung along the north side of the hole, which provided an orientation in the borehole.

The depths at which the fracture enters and exits the borehole were recorded as were the strike, dip, dip direction, aperture, and magnitude of the features.

The goal of the fracture analysis is to identify and model the major through-going structures that penetrate the LBT. This involved correlating the surface fracture traces with the location of fractures intersecting the boreholes. Correlation of the borehole fractures with the surface

fractures is confirmed by the location and the strike and dip of the fracture as measured in the video log.

Table 4-1. Number of Fractures Per Each Length Interval and the Percentage of Fractures Occurring in Each Interval

Number of fractures	Length (m)	Percentage	Cumulative percentage
1044	0.0–0.15	43.41	43.41
631	0.15–0.30	26.24	69.65
251	0.30–0.46	10.44	80.08
130	0.46–0.61	5.41	85.49
118	0.61–0.76	4.91	90.40
59	0.76–0.91	2.45	92.85
35	0.91–1.07	1.46	94.30
32	1.07–1.22	1.33	95.63
24	1.22–1.37	1.00	96.63
13	1.37–1.52	0.54	97.17
8	1.52–1.68	0.33	97.51
5	1.68–1.83	0.21	97.71
8	1.83–1.98	0.33	98.05
6	1.98–2.13	0.25	98.30
6	2.13–2.29	0.25	98.54
3	2.29–2.44	0.12	98.67
3	2.44–2.59	0.12	98.79
2	2.59–2.74	0.08	98.88
5	2.74–2.90	0.21	99.09
2	2.90–3.05	0.08	99.17
8	3.05–3.20	0.33	99.50
0	3.20–3.35	0.00	99.50
0	3.35–3.51	0.00	99.50
1	3.51–3.66	0.04	99.54
0	3.66–3.81	0.00	99.54
0	3.81–3.96	0.00	99.54
2	3.96–4.11	0.08	99.63
0	4.11–4.27	0.00	99.63
3	4.27–4.42	0.12	99.75
0	4.42–4.57	0.00	99.75
2	4.57–4.72	0.08	99.83
3	4.72–4.88	0.12	99.96
0	4.88–5.03	0.00	99.96
1	5.03–5.18	0.04	100.00

NOTE: Fractures mapped on all five sides.

Figure 4-3 is an equal-area diagram of pole to the major fractures that have been defined for the LBT. These fractures are defined by the surface mapping of the LBT and by the video mapping of the boreholes. Table 4-2 lists the major mappable fractures that have been modeled in the LBT. The individual modeled fractures are grouped into six fracture systems based on similarity in strike and dip. Figure 4-4 is a 3-D perspective of these six systems cutting the block.

Table 4-2. All Major Fracture Planes That Have Been Modeled for the LBT

Number	Strike	Dip	System number
LBT21	N32E	82NW	1
LBT11	N49E	43NW	1
LBT22	N52E	58NW	1
LBT2	N30W	78NE	2
LBT15	N37W	62NE	2
LBT14	N26E	01SE	3
LBT1	N36W	11NE	3
LBT30	N53W	09SW	3
LBT32	N68W	13NE	3
LBT31	N70W	09NE	3
LBT33	N78W	23NE	3
LBT38	N03W	89SW	4
LBT12	N04W	89SW	4
LBT16	N05W	89SW	4
LBT13	N10W	87SW	4
LBT37	N11W	88SW	4
LBT42	N16W	80SW	4
LBT36	N17W	87SW	4
LBT41	N18W	81SW	4
LBT20	N18W	87SW	4
LBT35	N18W	87SW	4
LBT6	N22W	78SW	4
LBT40	N25W	80SW	4
LBT5	N34W	77SW	4
LBT34	N70W	80SW	5
LBT8	N78W	79SW	5
LBT39	N78W	87NE	5
LBT3	N89E	90	5
LBT4	N46E	87SE	6

NOTE: These fractures are defined by the surface mapping of the LBT and by the video mapping of the boreholes.

Fracture system #1 is defined by three major fractures called LBT11, LBT21, and LBT22. This system occurs on the south and north sides of the large block and strikes N50E, then dips 40–45° to the northwest (Figure 4-5). System #2 consists of two major mapped fractures called LBT2 and LBT15. These fractures strike N30–40W and dip 60-80° to the northeast. The two fractures are mapped on the south and west sides of the large block (Figure 4-6).

Fracture system #3 contains six major mappable fractures. The fractures making up this system are LBT14, LBT30, LBT31, LBT32, LBT33, and LBT1, which is by far the most significant fracture in the LBT, because it completely cuts through the block and is identified in all vertical boreholes drilled from the top of the large block. As seen in the borehole videos, this feature generally has a wide aperture, common secondary mineralization, and, locally, alteration halos. These fractures are subhorizontal and have strikes that are generally northwest and dip about 20°

toward the southwest (Figure 4-7). These fractures occur on all four sides of the large block. The dip direction of these fractures is similar to the topographic slope of this part of Fran Ridge.

Fracture system #4 contains the greatest number of fractures. This system is defined by 13 major mappable fractures that penetrate the large block. The fracture attitudes range from N03 to 34W, dipping 77–89° to the southwest. This system is present on all sides of the LBT and contains a large number of subordinate, associated fractures with similar attitudes (Figure 4-8). Fracture system #5 contains three major mappable fractures that have a general east–west strike and near vertical dips (generally 80–90°) (Figure 4-9). Fracture system #6 is defined by two mappable fractures, LBT4 and LBT23. The fractures strike northeast with near-vertical dips (Figure 4-10).

Figure 4-11 is an equal-area net of poles to the major fractures that were mapped on top of the large block prior to construction of the LBT. The steeply dipping fractures correlate well with Figure 4-3, but the subhorizontal fractures are missing. These subhorizontal fractures were not observed in the initial mapping because of the shallow dip of the structures and probable subtle expression at the surface of the ground. This fracture pattern, including the subhorizontal fracture system, compares reasonably well with the fractures and faults that were mapped in the Climax Stock (Figure 4-12), located approximately 50 km northeast of Fran Ridge (Thorpe and Springer 1981, p. 14, Figure 6).

The fracture map of the ground surface above the area of the LBT prior to construction of the block is shown in Figure 4-13. The highlighted fractures have been identified in the large block and then projected to the land surface. Five of the six fracture systems have been identified; the subhorizontal fracture system #3 is not identified on this map. Identification and correlation of the fractures was done by projecting the measured attitudes of the LBT fractures up to the land surface.

Figures 4-14 through Figure 4-18 are 2-D presentations of all fractures mapped on the five surfaces of the LBT. The fracture systems are color-coded for increased visual discrimination.

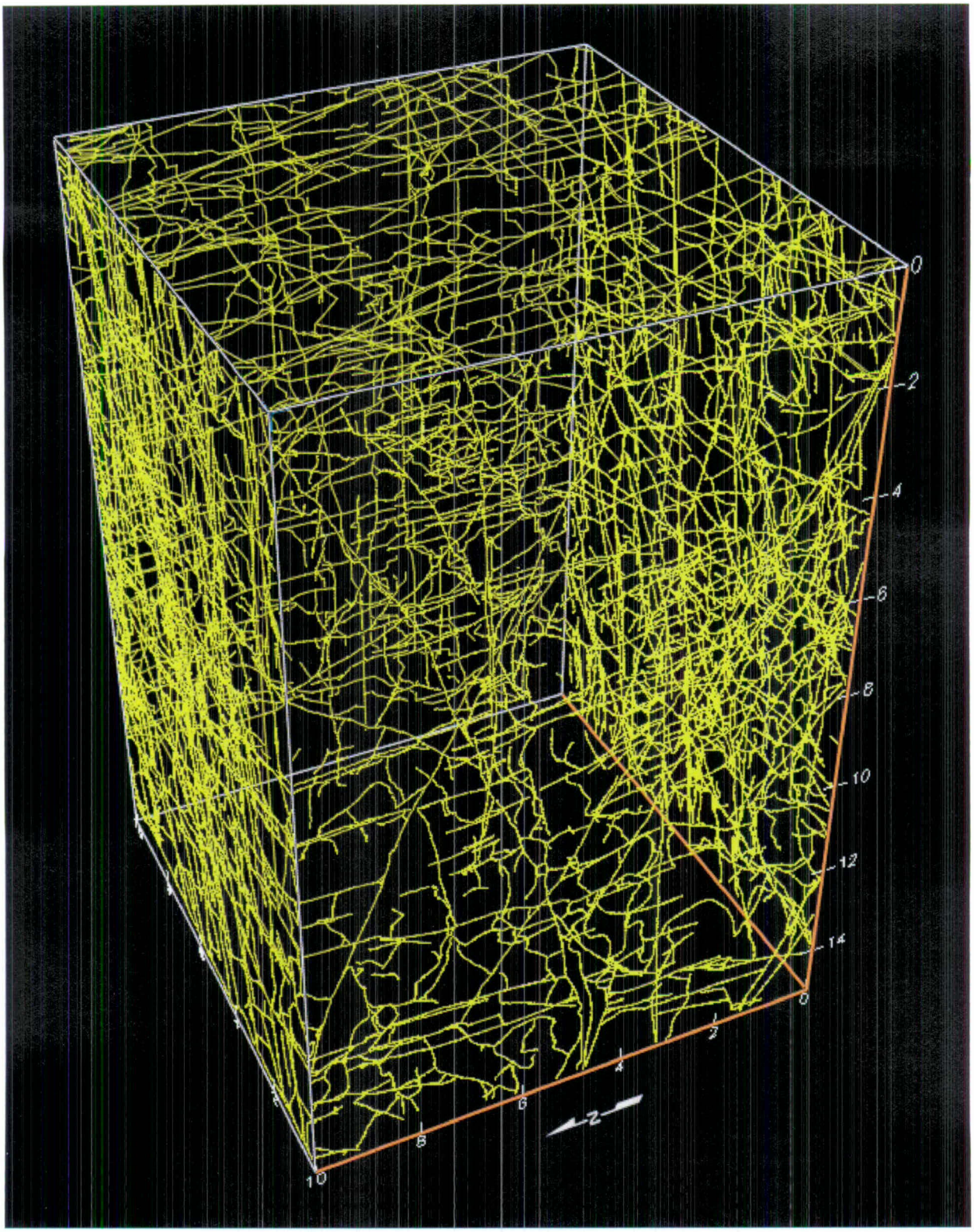

Figure 4-1. Mapped Surface Fractures on the Large Block

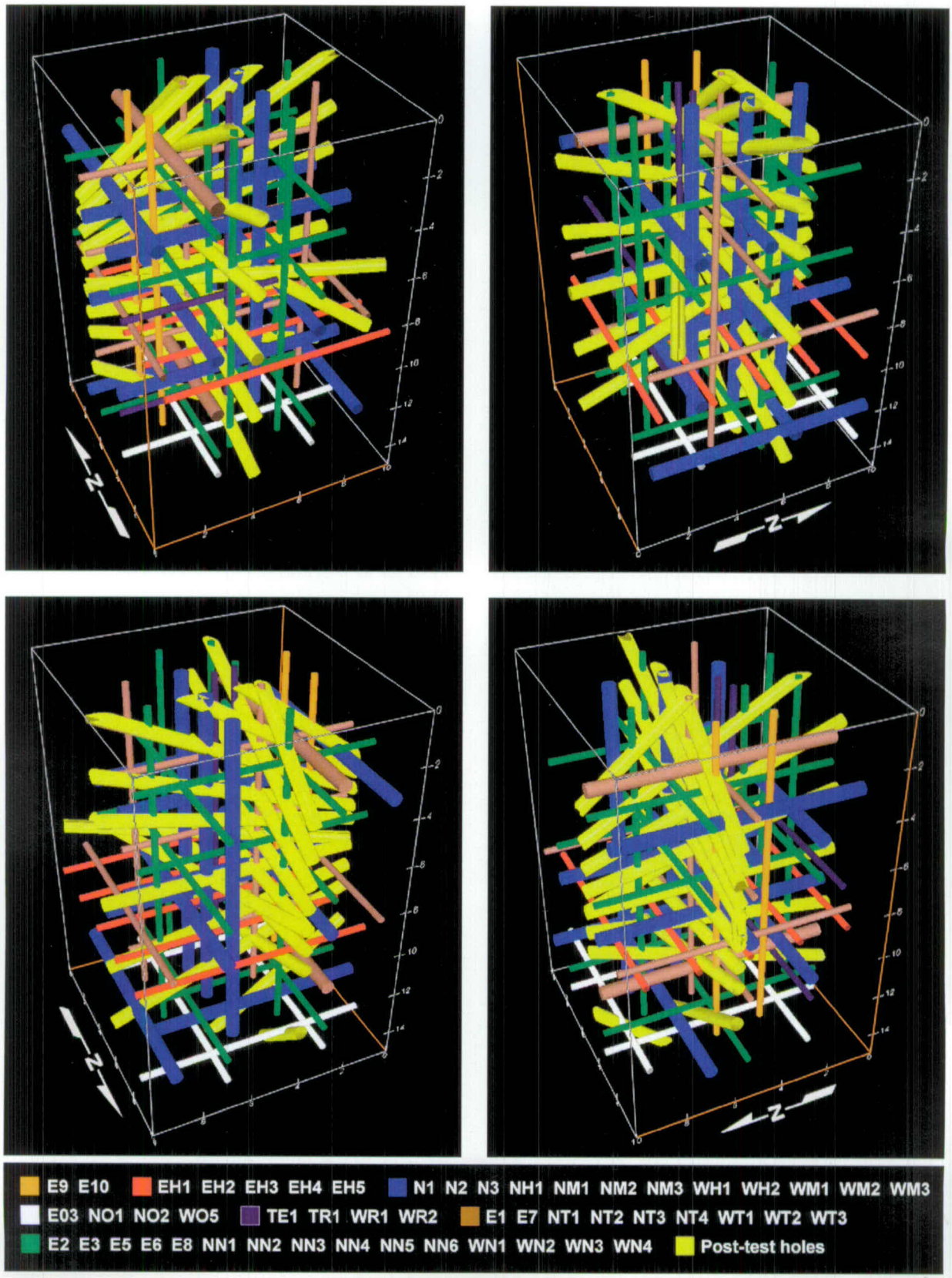

Figure 4-2. All Boreholes Drilled in the Large Block, Viewed at Various Angles

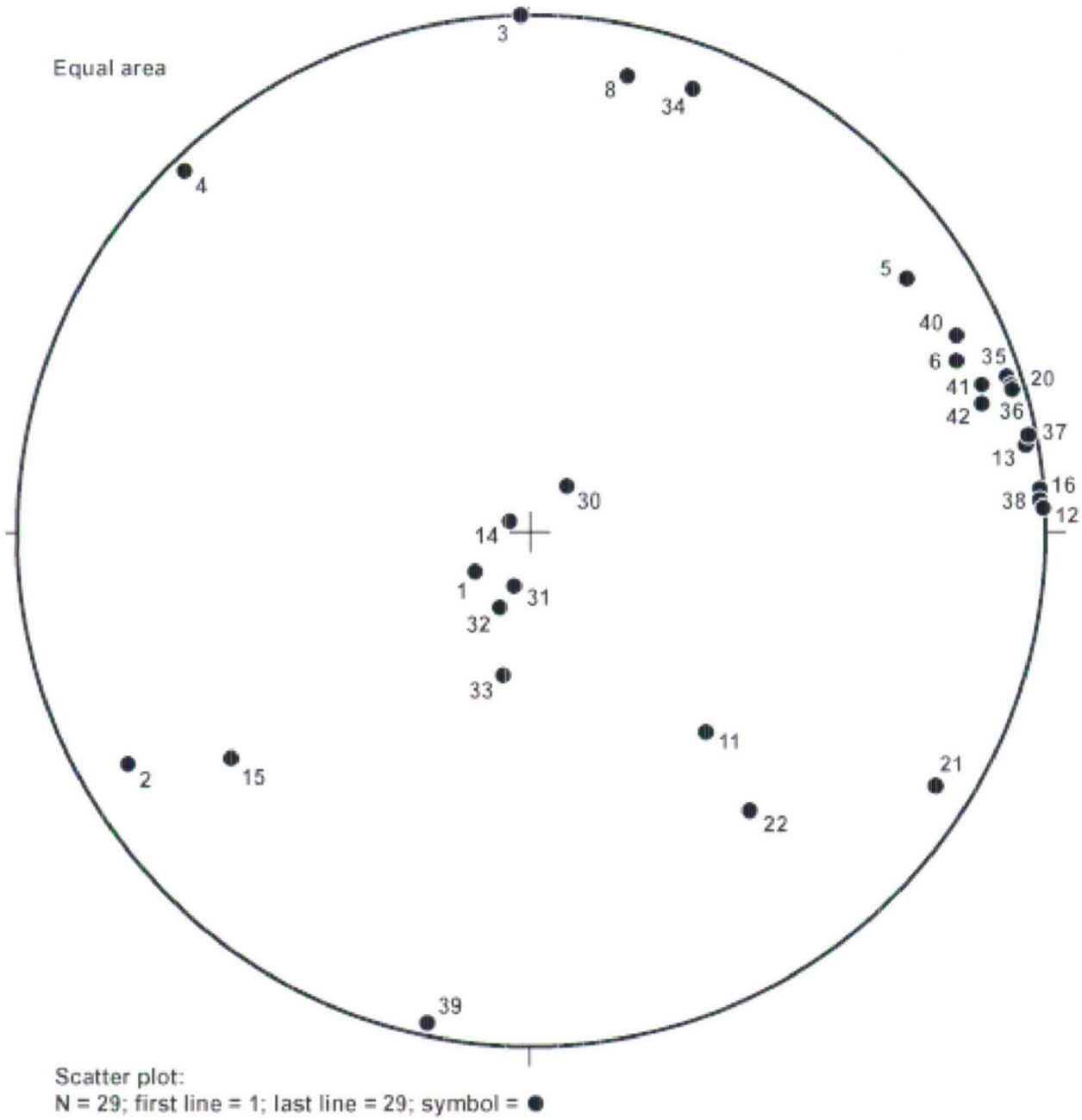

Figure 4-3. Equal-Area Diagram of Pole to the Major Fractures in the Large Block

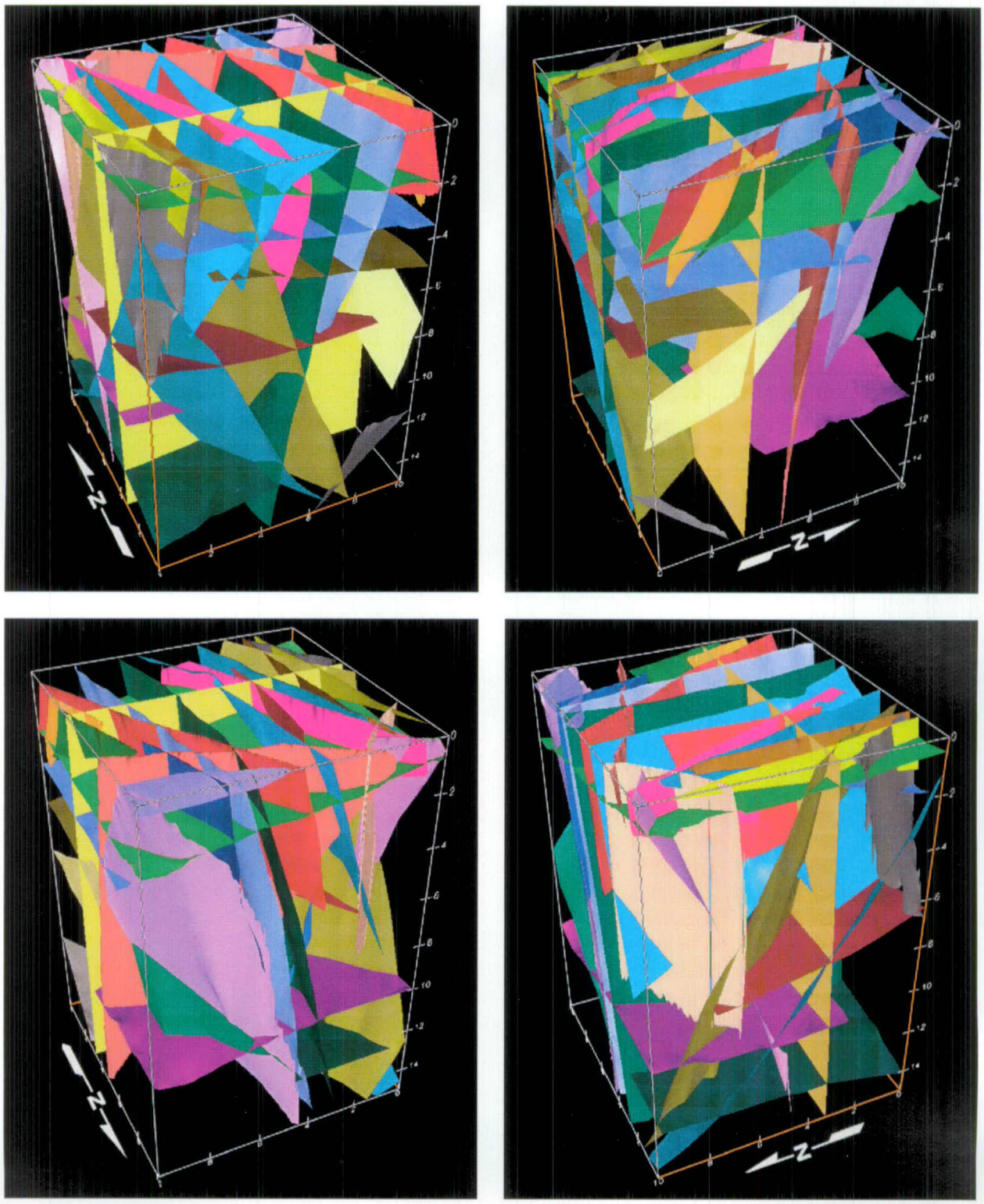

Figure 4-4. 3-D Depiction of the Major Mappable Fractures Cutting the Large Block

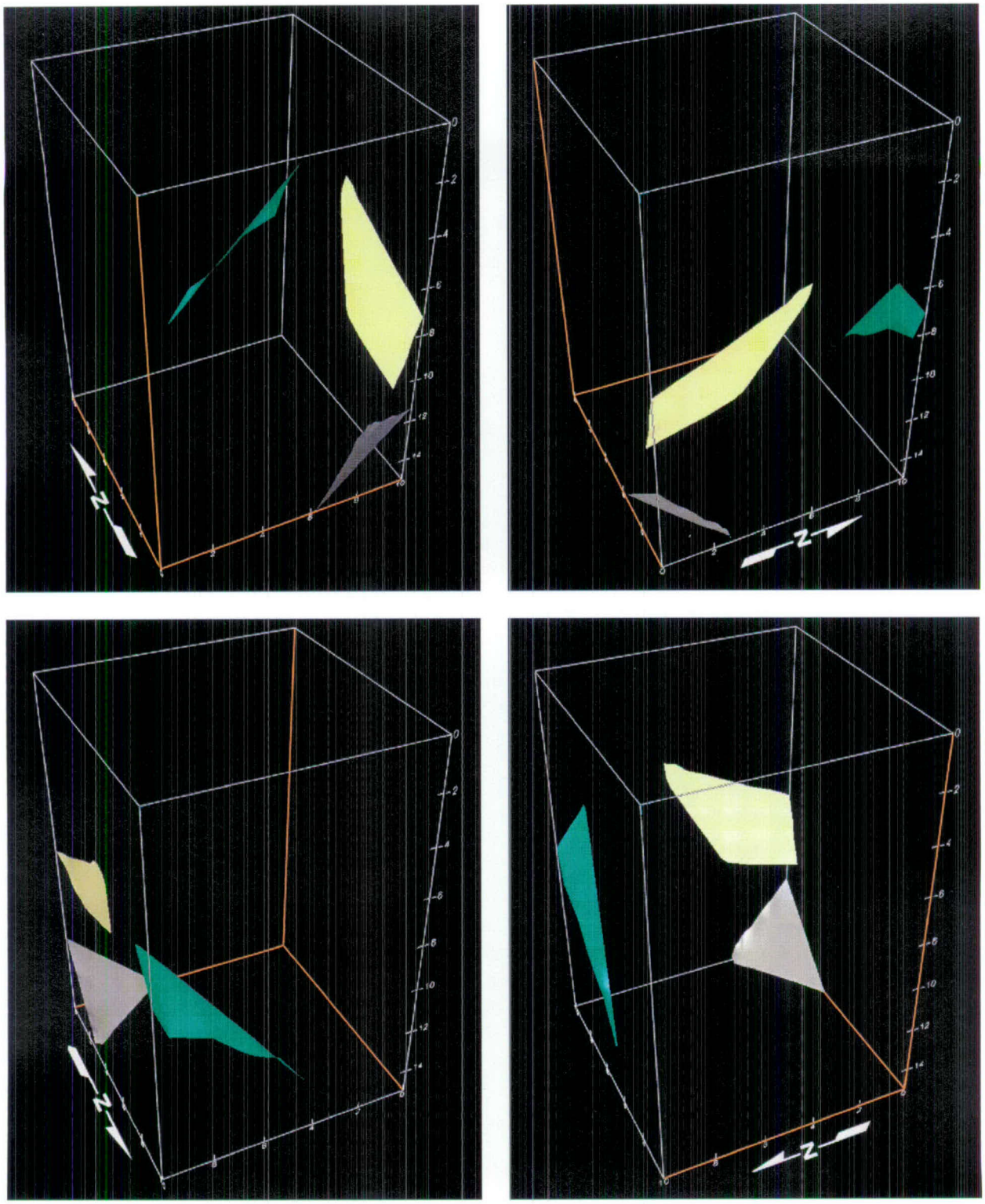

Figure 4-5. Fracture System #1 Contains Three Fractures That Strike N50E and Dip 40–45° Northwest

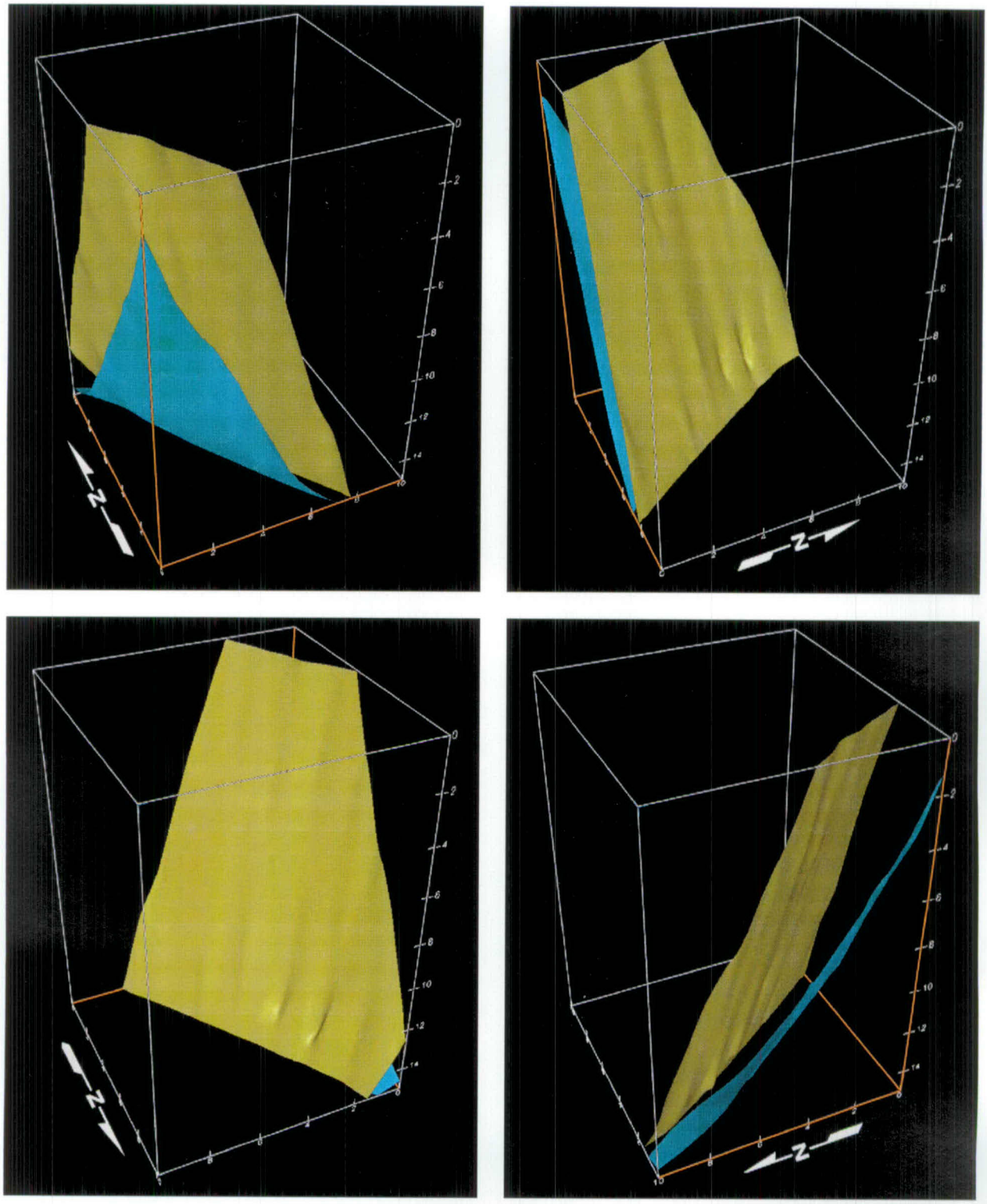

Figure 4-6. Fracture System #2 Contains Two Fractures That Strike N30–40W and Dip 60–80° Northeast

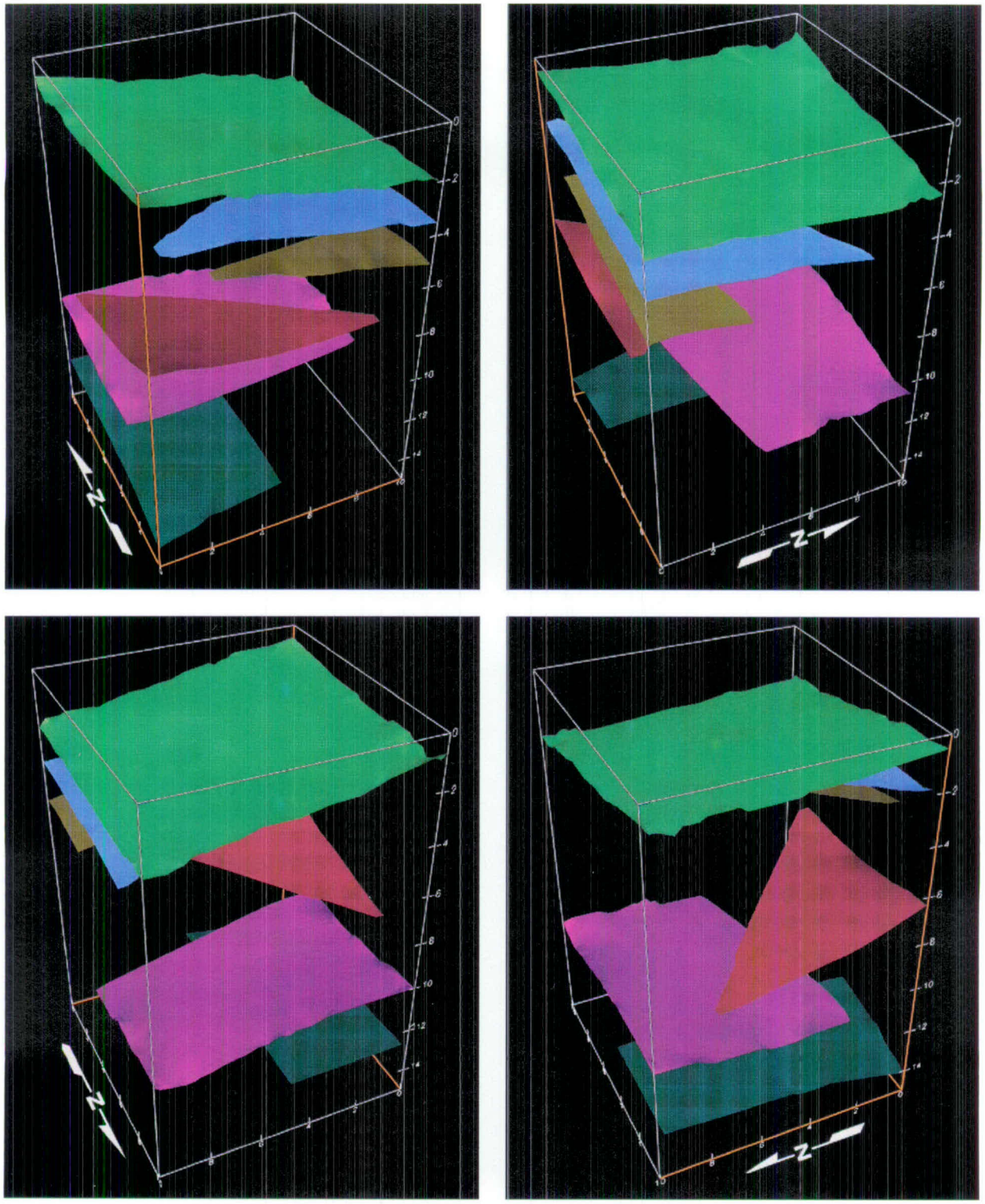

NOTE: Fracture LBT1 (green) is the largest, most significant fracture mapped in the block.

Figure 4-7. Fracture System #3 Contains Six Subhorizontal Fractures

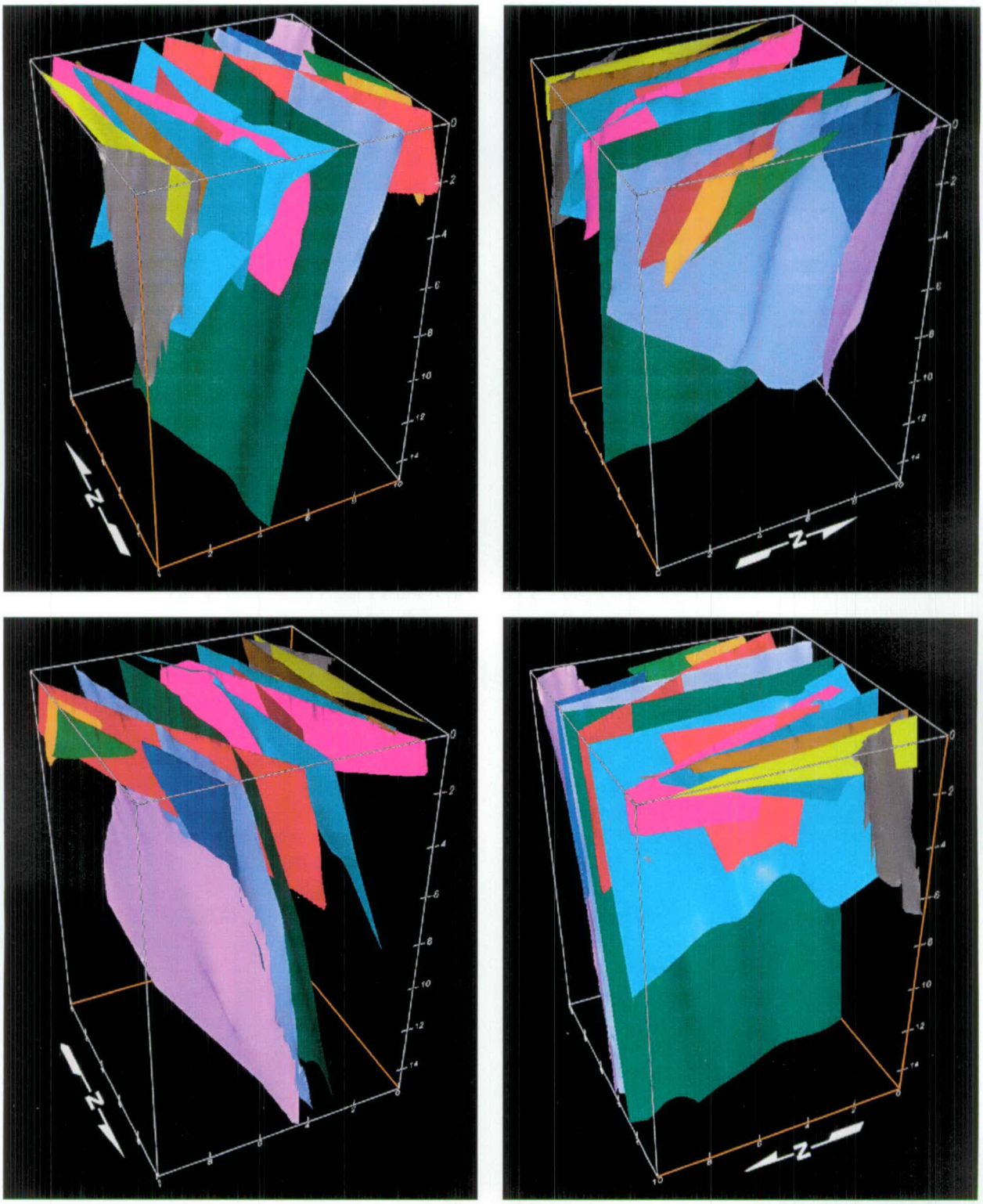

NOTE: This system strikes northwest and dips toward the southwest.

Figure 4-8. Fracture System #4 Contains 13 Mapped Fractures and Is the Dominant System in the Block

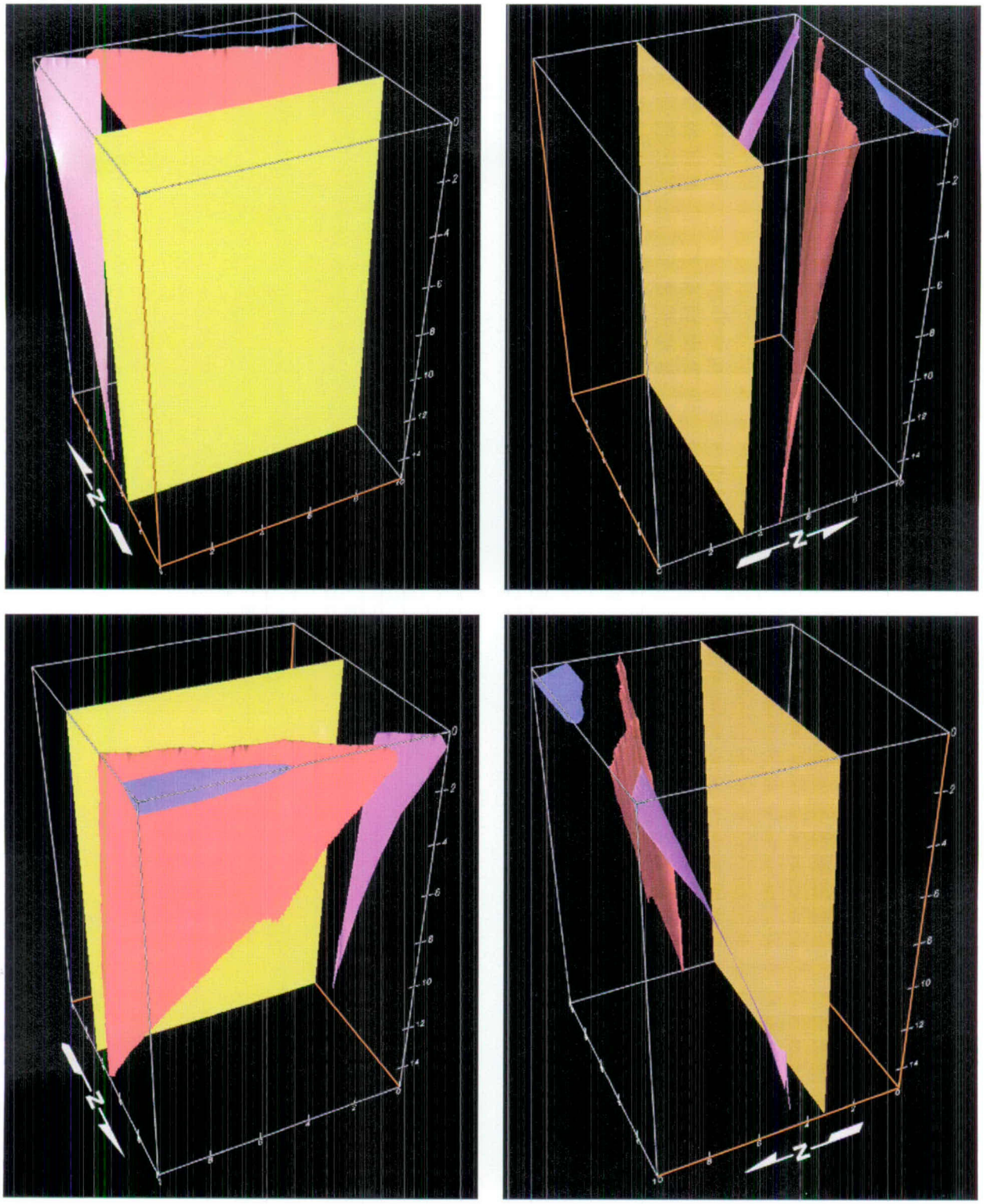

Figure 4-9. Fracture System #5 Contains Four Approximately Vertical Fractures That Strike East–West

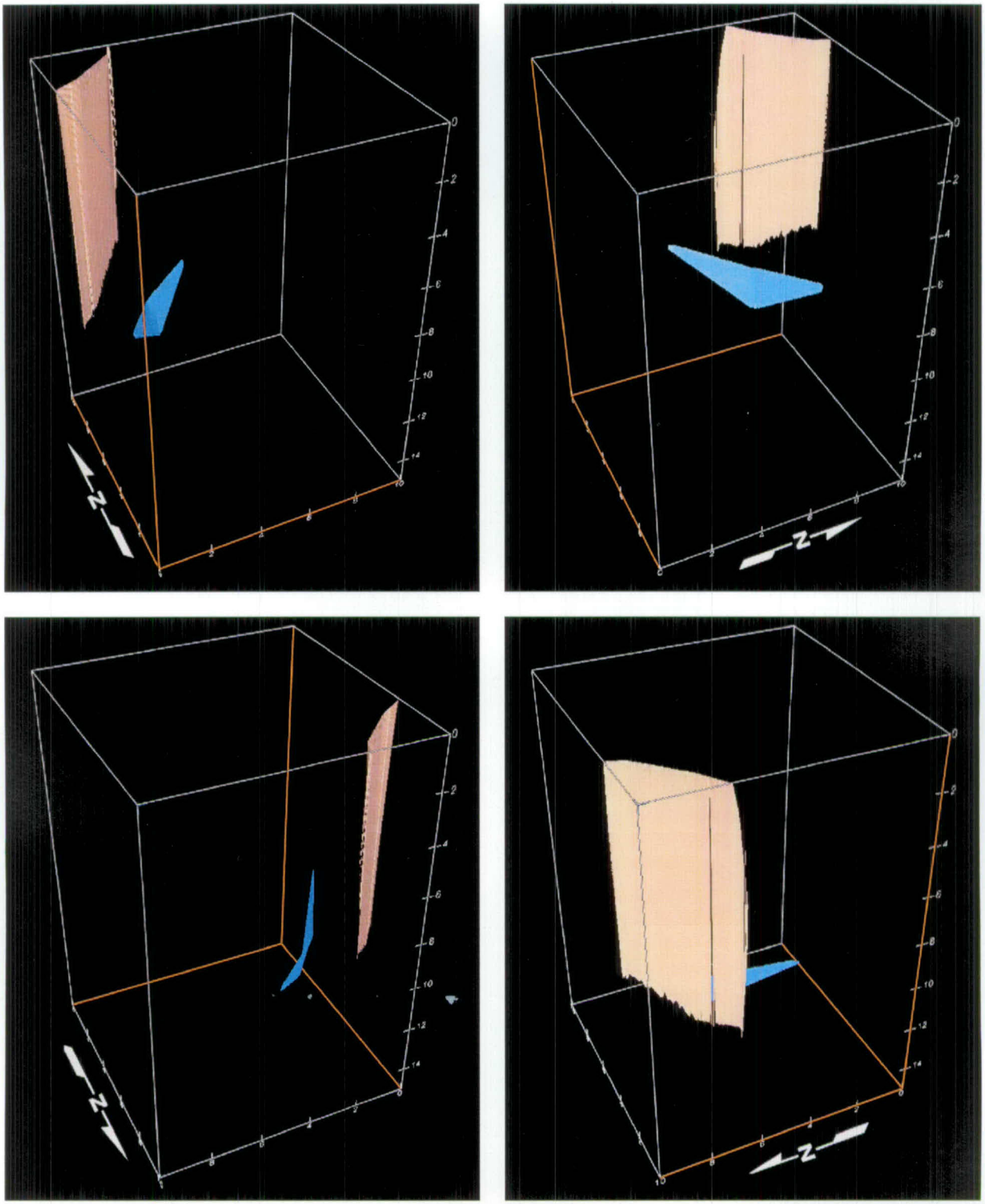

Figure 4-10. Fracture System #6 Contains Two Mappable Fractures That Strike Northeast and Dip to the Southeast

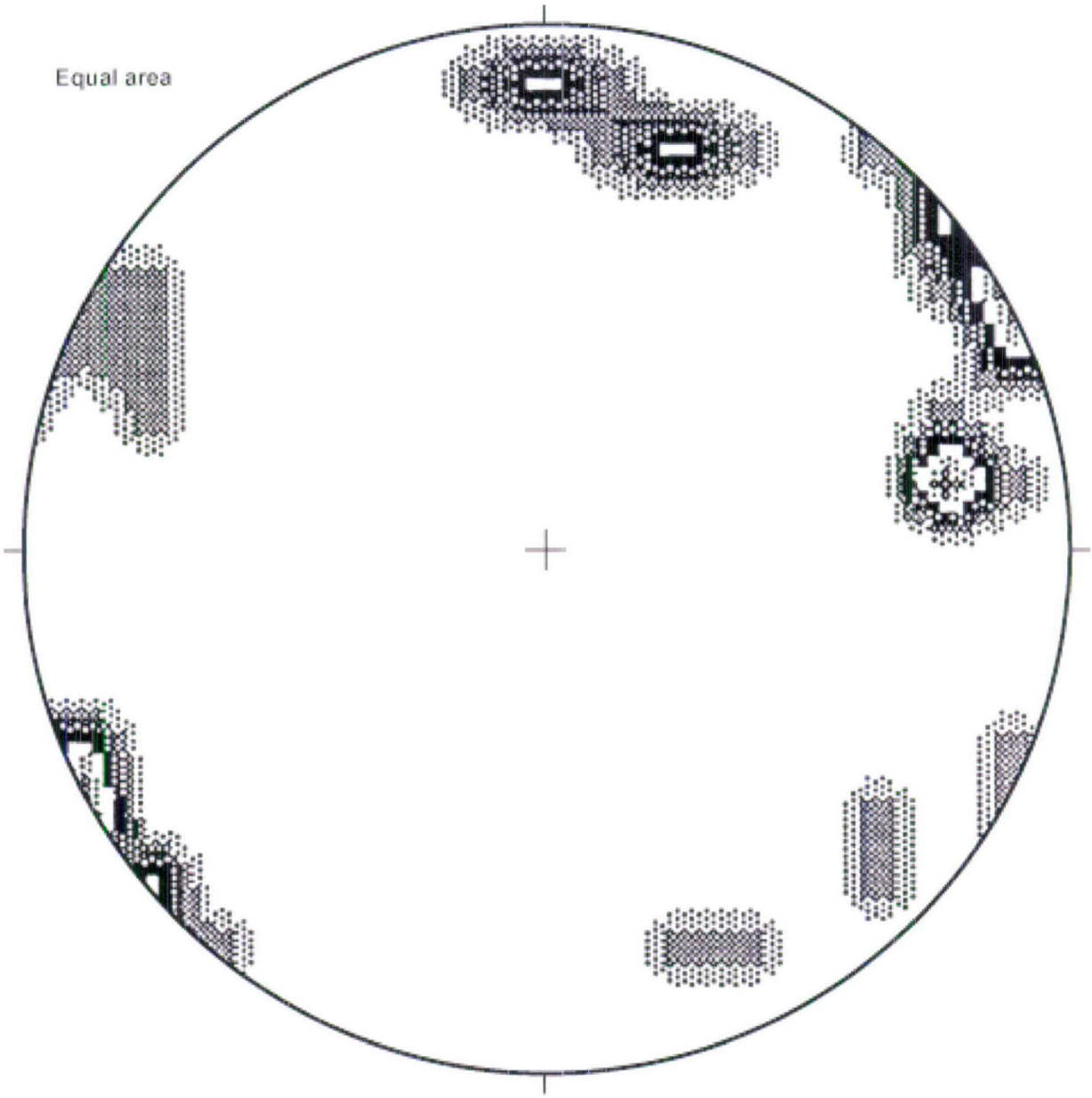

1% area contour:
N = 17; contour interval = 2%/1% area

Figure 4-11. Equal-area Net of Poles to the Major Fractures Mapped on Top of the Block

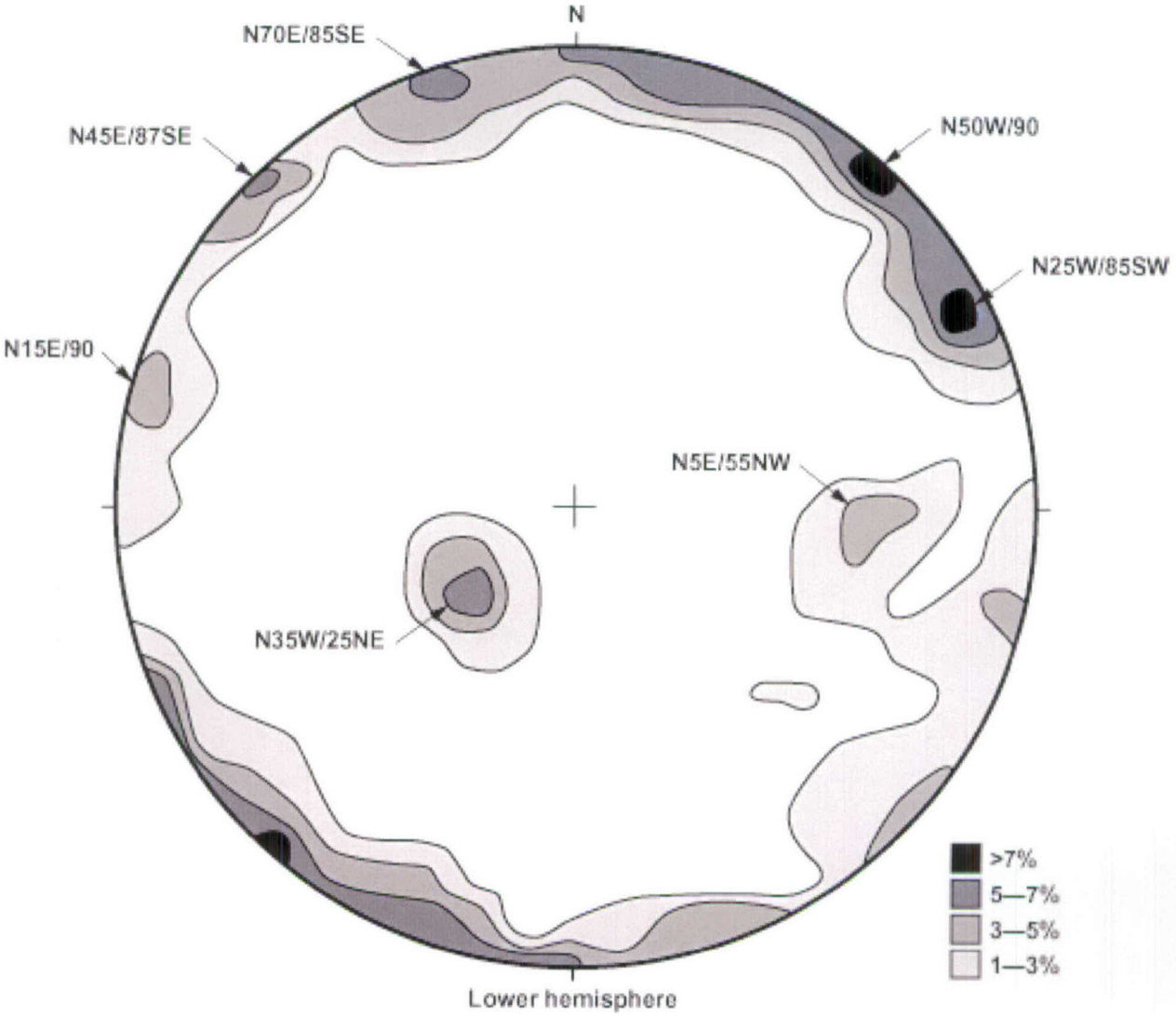

NOTE: Concentrations in percentage points within one percent area counting circle.

Figure 4-12. Equal-Area Contour Diagram of Poles to 90 Fractures Mapped in the Climax Stock Granite

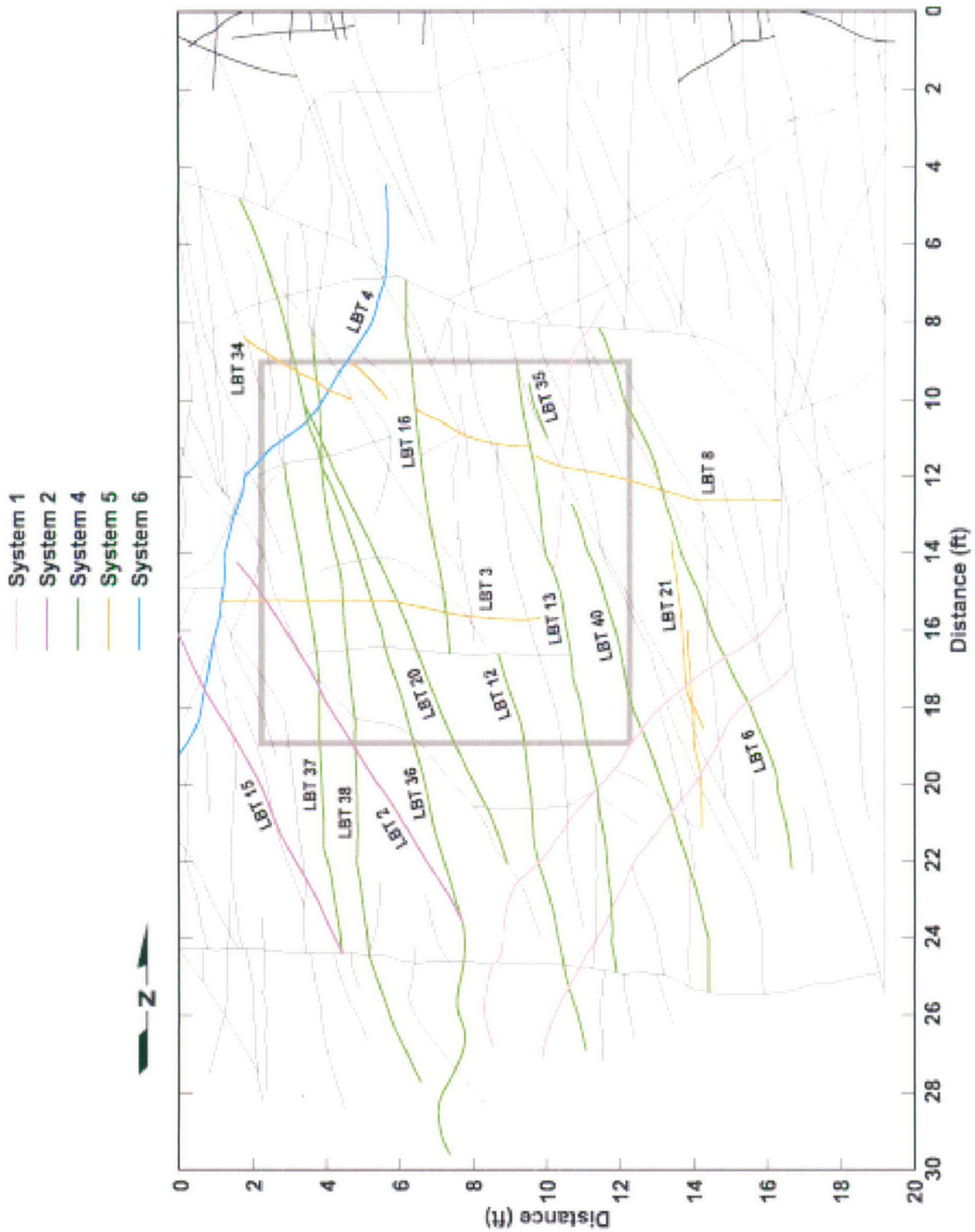

NOTE: Mapped LBT fracture systems were projected to this surface (color coded).

Figure 4-13. Fractures Mapped at the Fran Ridge Site Prior to Construction of the LBT (Square)

Figure 4-14. Mapped Fractures on Top of the LBT

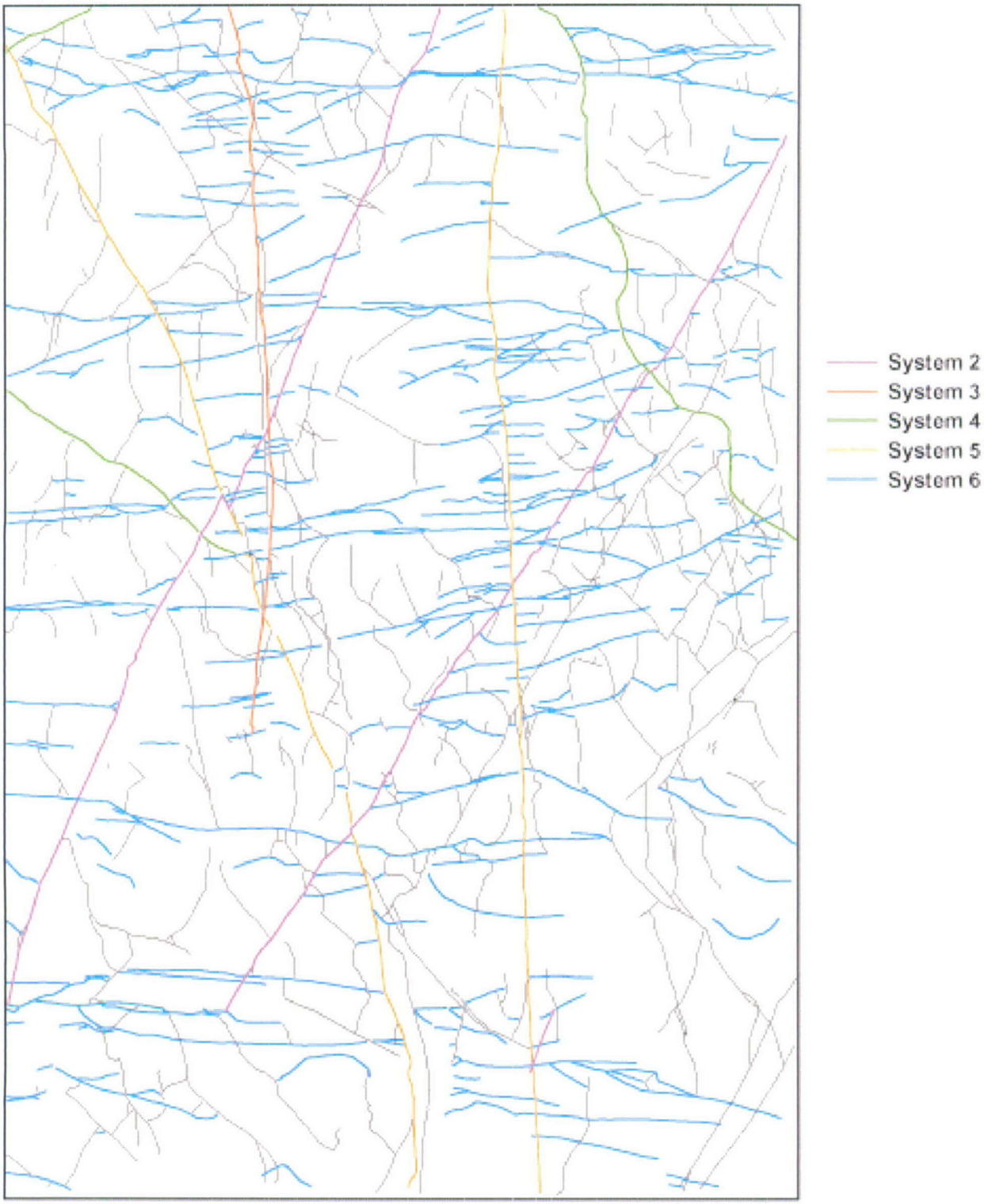

Figure 4-15. Mapped Fractures on the West Face of the LBT

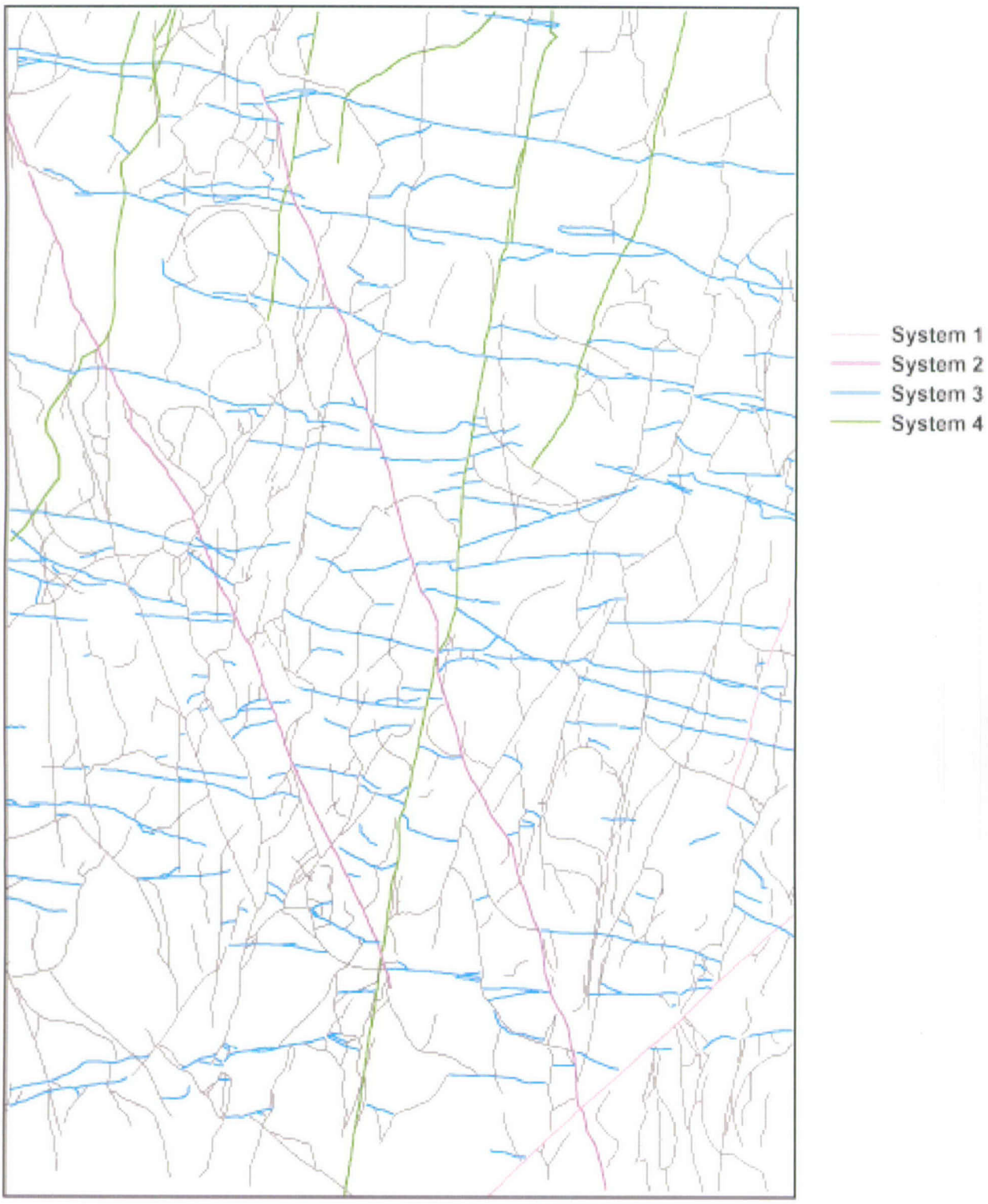

Figure 4-16. Mapped Fractures on the South Face of the LBT

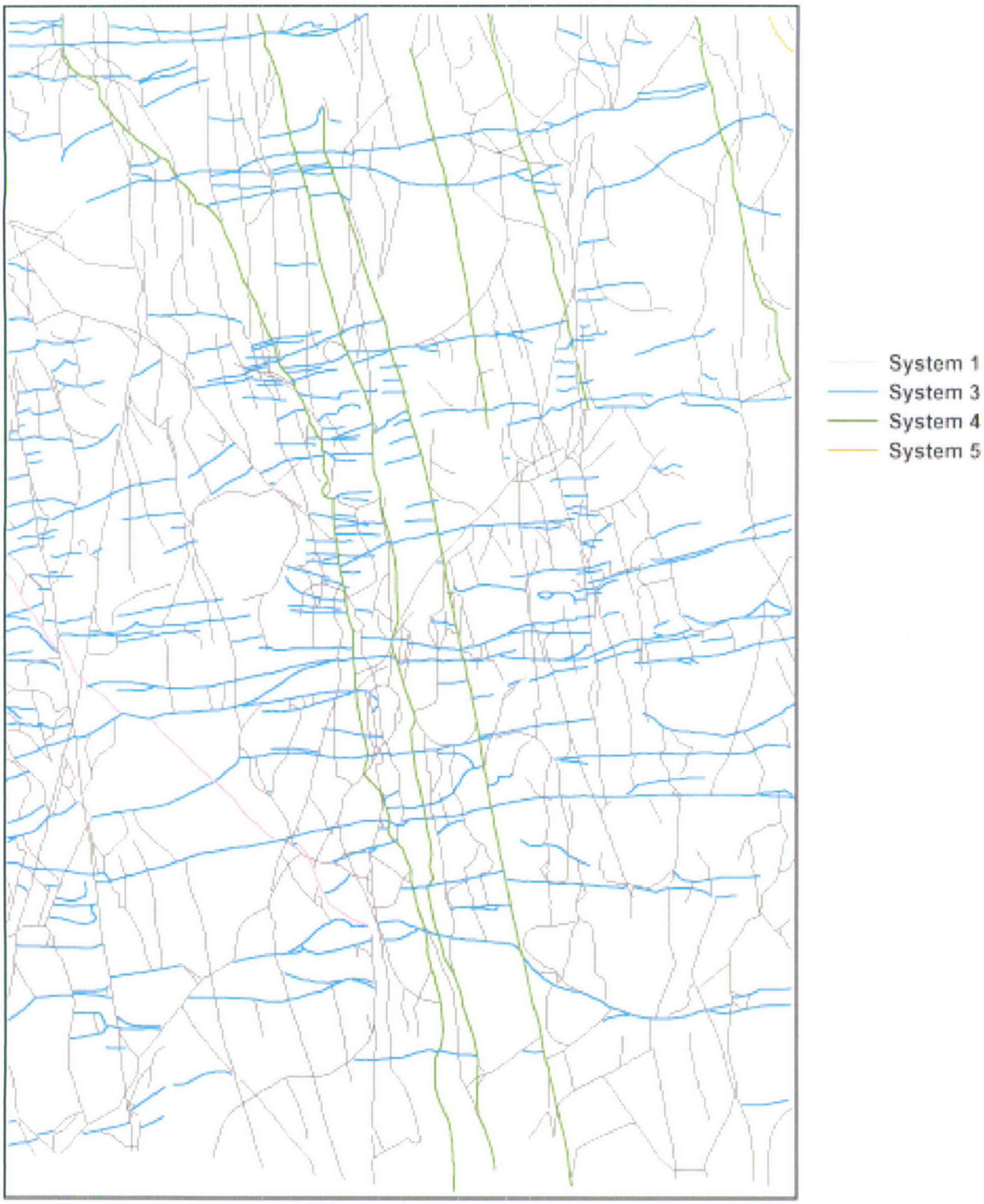

Figure 4-17. Mapped Fractures on the North Face of the LBT

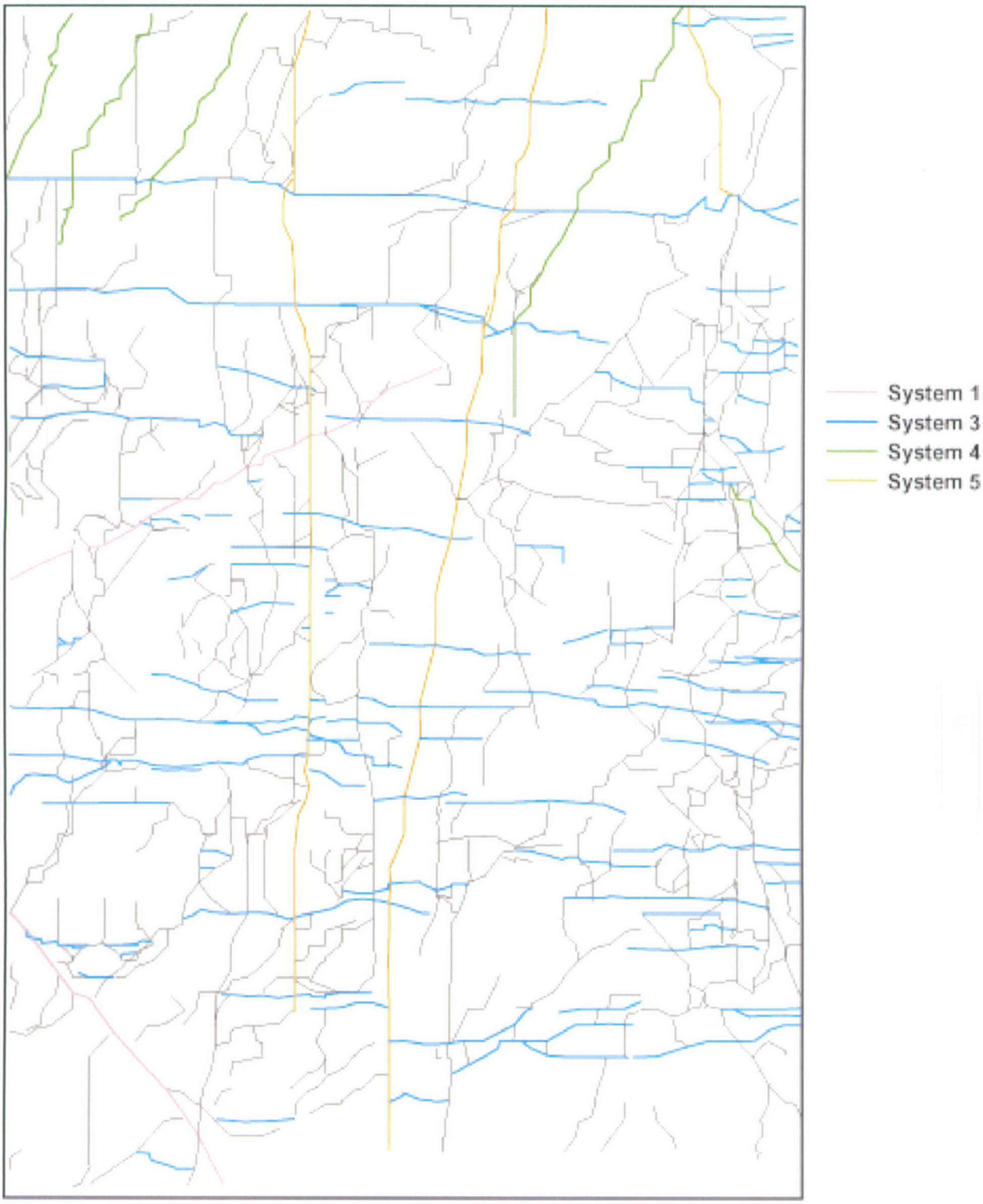

Figure 4-18. Mapped Fractures on the East Face of the LBT

5. THERMAL MEASUREMENTS

To impose and maintain a one-dimensional thermal gradient within the block, the block was outfitted with heaters in five boreholes in a horizontal plane and with a heat exchange unit on top. The heaters were 450 W each and were installed in each of the five horizontal heater holes. Heater temperature was monitored using three RTDs mounted to each heater.

5.1 LOCATION OF INSTRUMENTS

The instrumentation of the LBT is discussed in Section 3.3. The boreholes for the temperature measurement in the block are shown in Figures 3-7, 3-8, and 3-10.

5.2 BASELINE DATA COLLECTION AND HEATER TURN-ON

After all instrumentation was installed in the block and the moisture barrier and insulation were installed outside of the block, final characterization was completed with the cross-hole permeability and tracer tests described earlier. When the final characterization was completed, heaters and packers were installed (heater holes and hydrology holes had been used in the permeability and tracer tests), and baseline monitoring was initiated. Two weeks of baseline data were collected. Some instrumentation was able to take baseline data earlier, and nearly a month of baseline temperature data were collected. The heaters were then turned on February 28, 1997.

5.3 THE POWER OUTPUT FROM THE HEATERS

The heater in each of the five heater holes (EH1 to EH5 in Figure 3-9) was energized to 450 W on February 28, 1997. The power output of those heaters as a function of time is shown in Figures 5-1 to 5-5. The spikes in those figures were due to short-duration power outages. Those power outages did not affect the test significantly. The data gaps at 133 to 136 days and at 280 to 283 days were due to malfunction of the data acquisition unit. The power outputs of those heaters were about the same. The power was maintained fairly constantly with respect to time, at about 450 W until about Day 222, when the power was reduced in order to reach a steady-state temperature. The temperature at TT1-14 was maintained fairly constantly at about 135°C (see Figure 5-6) for the remainder of the test. During the later part of the test the power had to be increased back to almost the 450-W level in order to maintain a steady-state temperature. This was probably due to a cooler ambient temperature at that time.

5.4 TEMPERATURE OBSERVATIONS

Temperature in the block was measured using RTDs both in boreholes and on the surfaces of the block. As presented in Section 3.3, the borehole temperature measurements were conducted in 14 holes: two vertical holes (TT1 and TT2), seven horizontal holes (NT1, NT2, NT3, NT4, WT1, WT2, and WT3), and the five heater holes (EH1 to EH5). The temperature measurements on the top of the block were to verify that the heat exchanger controlled the top temperature at about 60°C during the test. The temperature measurements on the four vertical faces were for determining the thermal gradient on the surfaces, so that the heat flux away from the block could be determined. For the discussion of the temperatures within the block during the test, only the temperature measured in the boreholes will be used. The temperature measured on the block surface is discussed in Section 5.4.4. The two vertical RTD holes and the seven horizontal RTD

holes were sealed with grout during the test. The five heater holes were not grouted but were plugged at the collar using insulation material. In this report, only the temperature measured in the nine sealed RTD holes are presented in figures to illustrate the thermal responses of the block due to heating. As mentioned in Section 3.3, the RTDs in those holes were separated by a spacing of 20 cm. The RTD numbering was always starting from the bottom of a hole. For example, TT1-1 is the RTD at the bottom of the vertical RTD hole TT1, and NT1-14 is the RTD near the collar of the horizontal RTD hole NT1, which was drilled from the north face of the block and ended at a distance of about 30 cm from the south face of the block. All of the temperature data are available in Microsoft Excel spreadsheet form in the Technical Data Management System (TDMS) of the Yucca Mountain Site Characterization Project (YMP) and in the LLNL Large Block Test database. The DTNs for the data in the TDMS are listed in Table 1-1. The five heaters of the LBT were energized at about 10 a.m. on February 28, 1997, to a power level of about 450 W each. The preheat ambient temperature in the block was collected about 18 hours before the heaters were turned on. The data collection frequency was once per hour. The data acquisition frequency was increased to once per 10 minutes on June 30, 1997, in order to have a more accurate monitoring of the temperature fluctuations, which started on June 12, 1997, because of a TH event. The TH event is discussed in greater detail later in this section.

5.4.1 The Temperature History in the Block

The temperature in the two vertical RTD holes will be used to illustrate the temperature history in the block during the test. Figures 5-6 and 5-7 show the temperature history in holes TT1-14 and TT2-14 respectively. TT1-14 and TT2-14 are at 5 and 10 cm below the heater plane respectively. The location of holes TT1 and TT2 can be found in Figure 5-1. The temperatures at TT1-14 are about 10°C greater than those at TT2-14. This is mainly because TT1-14 is about 5 cm closer to the heater plane than TT2-14. All of the sharp drops in temperature that occurred before 100 days since heating are related to power outages. The short straight-line segment at about Day 135 was due to a temporary malfunction of the data acquisition system. TT1-14 represents the highest measured temperature in the rock of the LBT.

As shown in Figure 5-6, the temperature at TT1-14 increased with time rapidly at the early stage of the heating. The temperature increased with time mainly due to the conduction of heat from the heaters. The increasing rate of the temperature decreased with time, mainly due to the decrease of the thermal gradient at the RTD location as the thermal front expanded with time. A minor factor that also contributed to the decrease of the temperature rate is the consumption of energy in the evaporation of the in-situ pore water in the rock. When the temperature reached the boiling point of water, which is about 96.6°C at the elevation of Fran Ridge, the temperature rate of increase was significantly decreased. This was caused by rapid evaporation of the pore water in the rock. During the 20-day period between Day 30 and Day 50, the temperature at TT1-14 increased from about 96–98°C, indicating a very rapid evaporation but not boiling. After Day 50, the temperature at TT1-14 increased faster with time, indicating that most of the pore water had been evaporated. Then at Day 104 (June 12, 1997) the temperature dropped to near the boiling point of water. This is the on-set of the first of the two TH events, which are discussed below. The second TH event occurred at Day 186 (September 2, 1997). On Day 220 (October 6, 1997) the heater power started to ramp down, in order to keep the TT1-14 temperature at about 135–140°C. The heaters were turned off on March 10, 1998, to start a natural cooling phase. The data acquisition was terminated on September 30, 1998.

Figure 5-7 shows a very similar temperature history at TT2-14 to that of TT1-14, except for the apparent boiling of the pore water. The temperature at TT2-14 remained at 97.4°C for about 37 days (Day 75 to Day 112). Then the temperature increased to, and remained at, about 98.8°C for 16 days. This indicates that a process very close to boiling of the pore water was maintained at TT2-14. If boiling had actually occurred, the boiling point of the pore water is greater than the expected boiling point of pure water at the elevation of Fran Ridge (96.6°C). The greater boiling point of the pore water may be caused by the dissolved solutes in the water, and the increased pore pressure caused by the increased vapor pressure before the boiling. The increase of the boiling point of water during the boiling process (from 97.4 to 98.8°C) may be caused by the increased concentration of the solutes. In addition to boiling, another factor that may contribute to the constant temperature is a cooling effect by continuous flow of fluid to balance the energy. The mechanisms of maintaining such a continuous flow remain to be determined. Because the temperature at TT2-14 was at the boiling point of water when the first TH event occurred, the temperature at TT2-14 was not affected by that event. The rest of the temperature history at TT2-14 was very similar to that at TT1-14.

5.4.2 The Spatial Temperature Distribution in the Block

As mentioned in Section 3.1.1, the LBT was designed to perform one-dimensional heating of the block. Figures 5-8 and 5-9 show the temperature distribution along the two vertical RTD holes TT1 and TT2 respectively. To avoid cluttering the figure, only quarterly (since the heating) temperature snapshots are presented. As shown, the temperature was the highest at the heater plane and decreased with respect to distance away from the heater in both directions. The spatial temperature distribution in the vertical direction agrees well with the pre-test predictions, such as those shown in Figure 3-26.

Figures 5-10 through 5-16 show the spatial temperature variation in the seven horizontal RTD holes: NT1, NT2, NT3, NT4, WT1, WT2, and WT3 respectively. They show the horizontal spatial temperature variation in the block. The data gaps in Figures 5-11 and 5-16 are due to malfunction of RTDs NT2-9, NT2-13, and WT6. Generally speaking, the horizontal temperatures are fairly uniform in most parts of the block. The heating of the block was very close to one-dimensional.

All of the temperature data were input to EarthVision v5.0 to construct a 3-D contour of the temperature field within the block at certain instances. Figure 5-17 shows one example of such a temperature field in the block on March 10, 1998, before the end of the heating phase. This figure shows the temperature contours in a vertical cross section along TT1. With the 3-D temperature field, temperatures along any cross section in the block can be illustrated.

5.4.3 Temperature as an Indicator of Thermal-Hydrological Events

As shown in Figures 5-6 and 5-7, the temperature in the LBT illustrated two TH events on June 13, 1997, (Day 105.2) and September 2, 1997 (Day 186.5). There was no evidence that the June 13, 1997, event was associated with rain. It is known for certain that the September 2, 1997, event was associated with heavy rain, which had started the night before the event. The heat exchanger, which controlled the temperature on top of the block at about 60°C, was out of function for a few days starting on June 12, 1997 (Day 104.2). During the week from June 12, 1997 (Day 104.2) to

June 19, 1997 (Day 111.4), the temperature of the block top varied from 59°C to about 42°C, then back to about 59°C. During the September 2, 1997, event the heat exchanger functioned normally. The common features of these two events included: the temperature at some RTDs decreased sharply; the temperature at some RTDs increased sharply; the temperature at those RTDs near the heater plane tended to converge to the boiling point of water; the temperatures stayed at the boiling point of water for a while then increased with time sequentially, apparently when the rock began to dry out; and during the drying process the temperatures fluctuated with time with high frequency. However, there are differences between these two events, as discussed in the following paragraphs.

Figures 5-18 through 5-21 show the temperature along TT1 as a function of time during the June 13, 1997, event, (Day 105.2). At the beginning of this event, the temperature in TT1 at RTDs TT1-8 to TT1-12 increased (as shown in Figure 5-18); the temperature at TT1-13 to TT1-16 decreased (as shown in Figure 5-19); the temperature at TT1-17 to TT1-20 increased (as shown in Figure 5-20); and the temperature at TT1-24 and TT1-25 increased and the temperature at TT1-26 to TT1-28 decreased (as shown in Figure 5-21). The temperature at TT1-26 to TT1-28 was probably influenced by the malfunction of the heat exchanger. The temperatures at the RTDs below TT1-7 were not affected by this event. The different responses of the RTDs in TT1 show that this event was not strongly influenced by an exterior cause, such as rain water. Figures 5-19 and 5-20 show the main feature of this event: that is, the temperatures converged to near the boiling point of water, stayed at the boiling point of water for at least 14 days, then increased one by one, starting with TT1-14, which was closest to the heater plane. The increase of temperature with time, after staying at the boiling point of water, was probably due to the drying of the rock. When the temperatures were increasing with time, they fluctuated with high frequency. The temperature fluctuations extended beyond the time frame shown in the figures. The temperature fluctuation seemed to follow a similar sequence as the drying, because the temperature fluctuation at RTDs TT1-18 and TT1-23 extended into early September 1997. It was verified that the temperature fluctuation was not due to noise from the data acquisition system. Switching TT1-19 to a standard resistor on site did the verification; after the switch, TT1-19 read the resistance correctly. The temperature fluctuation was probably due to the reflux of the steam/water along the RTD column.

The influence of the June 13, 1997, event on the temperature in TT2 was not great. At the onset of the event, there was almost no significant variation in the temperature in TT2. The temperature at several RTDs in TT2 (TT2-13 to TT2-20) associated with the fluctuation as in TT1, but with much less amplitude, until September 1997. One of the possible causes of this event is that some mechanical effect caused the release of the overheated pressurized water to flow quickly along the RTD column in both TT1 and TT2. The location of this release of the pressurized water is not known but was maybe somewhere above the heater plane. When the water was released, its temperature decreased quickly but was still near the boiling point of water. The water could flow both upward (due to pressure gradient) and downward (due to both the pressure gradient and the gravity). The quick flow of this boiling water caused the temperatures along the RTD column to change. The boiling/rapid evaporation of this water caused the temperature to stay at near the boiling point of water for an extended period. Then the steam/condensate refluxing caused the temperature fluctuations.

Figures 5-22 through 5-25 show the temperatures in TT1 as a function of time during the September 2, 1997, event (Day 186.5). Figure 5-22 shows that at the onset of the event the temperature at TT1-11 decreased; there was a slight increase at TT1-9 and TT1-8; there were no changes in the temperature at the RTDs below TT1-7. Figures 5-23 through 5-25 show that at the onset of the event (Day 186.5), the temperature at all RTDs decreased then increased, except at TT1-19, where the temperature only showed the later increase. This feature was different from that in the June 13, 1997, event. This is an indication that the September 2, 1997, event was strongly influenced by an exterior source, such as rain. The effect of this event on the temperature in TT2 is similar to that on TT1. Figure 5-22 shows the main feature of this event. The temperatures converged to near the boiling point of water, similar to the June 13, 1997, event, and stayed at that temperature for about two days only. This "boiling" period was much shorter than that of the June 13, 1997, event. The temperatures then began to increase in the order of distance from the heater plane, again similar to the June 13, 1997, event. The temperatures fluctuated with time after the boiling period, also similar to the June 13, 1997, event. Despite the apparent difference in the cause of the event, the TH feature of this event is very similar to that of the June 13, 1997, event. The shorter "boiling" period in this case was because the rock mass was dry when this event occurred, and the rain provided most of the water, which drove the event. Another reason for the quicker drying out was because more insulation was put on the block surface before the event; therefore, more heat was available for the drying. Figure 5-25 shows that steam coming from below was enough to maintain the temperature at TT1-24 to TT1-28 at the boiling point of water for a few days. When the steam was gone, the temperatures decreased one-by-one, starting from the top. Most of the temperature fluctuations stopped by September 17, 1997 (Day 201.4), but the temperature at TT1-23 fluctuated until October 20, 1997 (Day 234.4). The effect of this event on the temperature in TT2 is very similar, with smaller amplitudes of the temperature fluctuations. The process of this event was similar to that of the June 13, 1997 event, but the cause was the rainstorm in the night before.

5.4.4 Heat Flux on the Block Surface

As mentioned earlier, the surface temperature of the block was measured in zones. The four vertical faces of the block were divided into four zones (1 to 4) from bottom to top. The first three zones were 1.219 m in height. The fourth zone (near the top) was about 0.762 m in height. Each face within each zone was further divided into three regions: one central region and two corner regions. The central regions were designated as N1 to N4, W1 to W4, E1 to E4, and S1 to S4. For example, N1 to N4 were for the central region in the north face, for zones 1 to 4 respectively. The corner regions were designated as NW1 to NW4, NE1 to NE4, SW1 to SW4, and SE1 to SE4. For example, NW1 to NW4 represented the north-west corner for zones 1 to 4 respectively. Each corner region included a portion of both faces that formed the corner. For example, NW1 included a portion of the north face at the corner and a portion of the west face at the corner, in zone 1. The central region of zones 1 to 3 in each face was about 2.438 × 1.219 m. The corner regions of zones 1 to 3 in each face were 0.305 × 1.219 m each. In the zone 4, the central region in each face was 2.438 × 0.762 m, and each of the corner regions was 0.305 × 0.762 m. Within each region, two RTDs were mounted on the both sides of Ultratemp insulation sheet, which was then mounted against the vertical face of the block. In the corner regions, only one pair of RTDs were mounted. The RTD pair might be mounted on either side of the corner.

For example, the RTD pair in NW1 might be mounted either on the Ultratemp insulation sheet of the north face or the west face.

Those surface temperatures were used to obtain the temperature field within the block, along with the temperatures measured in boreholes discussed earlier. The surface temperatures were also used to calculate the heat flux from the block during the test. The thermal gradient normal to the block face in each region was calculated by dividing the temperature difference, measured by the RTD pair, by the thickness of the Ultratemp sheet. The heat flux was calculated by multiplying the thermal gradient with the thermal conductivity of the Ultratemp. The thermal conductivity of the Ultratemp was provided by the manufacturer as 0.093 W/m-K. The heat flux data can be used in TH modeling to account for the energy balance.

Figures 5-26 through 5-29 show some examples of the heat flux from the block as a function of time, in zones 1 to 4 respectively, during the steady-state temperature period (February 8–25, 1998) of the test. It is expected that the heat flux was dependent on the temperature in the block. Zone 2 included the heater plane and therefore had the greatest heat flux in all regions. The north-west corner had the greatest heat flux in both zones 1 and 2. This was probably related to a greater fracture intensity near the north-west corner than in other places in the block. Besides NW2, S2 had greater heat flux than other regions in zone 2. (There was no good data for W2.) This was probably due to more fractures intersecting the south face than the north and east faces in this zone. In zones 3 and 4 the heat flux was about the same in all regions. The nonuniform heat flux may have to be considered in order to fine-tune a TH model.

5.5 THERMAL CONDUCTIVITY AND THERMAL DIFFUSIVITY

As presented in Section 3.4.1.2, the thermal conductivity and thermal diffusivity of the block were measured in situ by using the REKA thermal probe method. The REKA method incorporated the application of three small probes (0.013 m in diameter and 0.125 m in length) that were cemented into the rock block. The probes were heated by built-in heaters of 4 W during the measurement period of 24 hours. When not activated, the probes were not heated.

Three permanent REKA probes were grouted into the large rock block at Fran Ridge. As shown in Figure 3-11, horizontal REKA Probe 1 was installed 0.584 m below the rock block's heater plane; horizontal REKA Probe 2 was installed 0.889 m above heater plane; and the vertical REKA Probe 3 was installed with its representative sensor location 1.38 m above the heater plane. Each probe reading approximately represents a 0.1-m-diameter spherical rock volume.

The measured temperature fields were evaluated using the REKA 01 software that was qualified in 1998 in accordance with the LLNL quality assurance (QA) program. The effective conductivity and diffusivity results (Danko et al. 1998) are shown in Figures 5-30 to 5-32 for the three REKA probes. Day 0 in Figures 5-30 to 5-32 denotes the time of the start of the heating of the block. As shown in Figures 5-30 to 5-32, both k and alpha values are varying only slightly with time. There is an apparent correlation between the variations of the in-situ, independently obtained conductivity and diffusivity values. This correlation indicates that the specific heat and the density (ρ) are approximately constant with time in the rock, since the equation

$$\rho \times c = {}^{k}/_{alpha} \qquad \text{(Eq. 5-1)}$$

has to be satisfied. Therefore, the variations can be attributed to the change in the convective effects with time, caused by moisture and/or vapor migration. The assumption that the conductivity and diffusivity values are affected by the heat-driven convective effects seems to be supported by the apparent correlation between the k, alpha, and rock temperature values, shown in Figures 5-30 through 5-32.

In summary, the results of the in-situ REKA probe measurements agree very well with the expected values at Fran Ridge (Nimick 1990). The REKA method is sensitive enough to detect convective effects. More advanced evaluations (Danko and Buscheck 1993) of the REKA measurements, using the NUFT hydrothermal model, are needed to quantify the TH effects upon the effective rockmass heat conductivity (k) and thermal diffusivity (alpha).

5.6 THERMAL-HYDROLOGICAL MODEL ANALYSES OF THE TEMPERATURE DATA

The TH processes of the LBT were modeled using NUFT 3.0.1s (STN 10130-3.0.1s-00) using the implicit dual-permeability model and the active fracture concept, as reported in Section 6.2.4 of the Thermal Test TH AMR (CRWMS M&O 2000c). The model analyses used two property sets: the drift-scale (DS) property set and mountain-scale (MS) property set, as shown in Table 5-1 (CRWMS M&O 2000c, Table 7). Although the LBT was not designed to test various property sets of YM, it is interesting to see how well the property sets work. Statistical analyses of the goodness of fit between the measured and calculated temperatures in the block were reported in the AMR cited above. This section presents the comparison between the measured temperatures in the block and the calculated ones. The comparison of the measured moisture content and the model calculation are presented in Section 6.2.2.

5.6.1 Numerical Model

The model geometry, boundary and initial conditions, and heater power history are identical to those presented in Section 6.2.4 of the Thermal Test TH AMR (CRWMS M&O 2000c) for the DS property set. The DTN for heater power histories used in the analysis is LL980918904244.074.

5.6.2 Rock Property Data Sets

Hydraulic and thermal properties of the tsw34 unit of the DS basecase property set (DTN LB990861233129.001) and the MS basecase property set (DTN LB997141233129.001) were used in model calculations. The tsw34 unit was used because the hydrogeologic unit of the LBT area is equivalent to the tsw34 model unit (Tptpmn) of the site-scale unsaturated zone (UZ) flow model. The only difference between the DS and MS properties for the tsw34 unit is a higher fracture permeability of 1.70×10^{-11} m^2 for the MS versus 2.76×10^{-13} m^2 for the DS. Properties of the LBT insulation for the simulations are also included in Table 5-1 (Table 7, Section 6.2.4 of the Thermal Test TH AMR [CRWMS M&O 2000c]).

Table 5-1. The DS and MS Rock Properties and the Thermal Properties of the Insulation Material Used in the TH Modeling of the LBT. (Source: Table 7 of CRWMS M&O 2000c)

Property	DS[a] Host rock (base case) and insulation	MS[b] host rock and insulation
Ultratemp thermal conductivity (W/m°C)	0.095[c]	0.095[d]
Ultratemp specific heat (J/kg°C)	1130[c]	1130[d]
Insulator thermal conductivity (W/m°C) (after 125 days)	0.05[c]	0.05[d]
Matrix permeability (m^2)	4.07×10^{-18}	4.07×10^{-18}
Fracture permeability (m^2)	2.76×10^{-13}	1.70×10^{-11}
Matrix porosity	0.11	0.11
Fracture porosity	2.43×10^{-4}	2.43×10^{-4}
Matrix van Genuchten αm (1/Pa)	3.86×10^{-6}	3.86×10^{-6}
Matrix van Genuchten βm	0.291	0.291
Matrix residual saturation	0.19	0.19
Fracture van Genuchten αf (1/Pa)	5.16×10^{-4}	5.16×10^{-4}
Fracture van Genuchten βf	0.608	0.608
Fracture residual saturation	1.00×10^{-2}	1.00×10^{-2}
Initial liquid saturation	75%[c]	75%[d]
Dry thermal conductivity (W/m-K)	1.56	1.56
Wet thermal conductivity (W/m-K)	2.33	2.33
Specific heat (J/kg-K)	948	948
Tortuosity	0.7	0.7
Gamma parameter for the active fracture model (γ)	0.41	0.41
Fracture frequency (m^{-1})	4.32	4.32
Fracture to matrix interface area (m^2/m^3)	13.54[c]	13.54
Grain density (kg/m^3)	2530	2530

NOTE: [a]DS (Drift-scale property set), DTN:LB990861233129.001
[b]MS (Mountain-scale property set), DTN:LB997141233129.001
[c]DTN:LL000321204242.092
[d]DTN:LL000314304242.094

5.6.3 Drift-scale Simulation Results Versus Field Data

Figure 5-33 shows the simulated versus measured temperature profile along Borehole TT1 at six times from 30 to 400 days. The DTN for all field temperatures data is LL970803004244.036. The model, with the DS property set, shows some overprediction of temperature at earlier times, but the difference between simulated and measured temperatures decreases at later times. At 300 and 400 days (25 days after power shutdown), the agreement is excellent.

Two statistical measures of goodness-of-fit, the root-mean-squared difference (RMSD) and mean difference (MD) between measured and simulated temperatures along Borehole TT1, were computed at various times from 30 days to 500 days. The results are tabulated in Table 5-2. As shown in the temperature profiles, the RMSD plot indicates a good fit between simulated and field temperatures. The match is good at 30 days, worsens at 100 days, and then consistently improves thereafter. The MD is always positive, which indicates that the DS data set, in general,

overpredicts the temperatures. Again, the accuracy of the prediction consistently increases with time after 30 days, reducing to a mean error of less than 1°C at 500 days, 125 days into the cool-down phase.

Figure 5-34 shows comparisons of simulated and measured temperature histories at two sensor locations, TT1-14 and TT1-19, in TT1. The temperature history at TT1-14 (2.76 m below the top of the block) matches the field data fairly well in the time ranges 0 to 25 days and 225 to 375 days. The model, using the DS property set, overpredicts temperature in the time range 225 to 375 days. The simulated cool-down lags the measured cool-down by a few degrees. Model overprediction, especially between 25 and 225 days, may reflect that the rock properties do not adequately match the field conditions at the LBT. The overprediction might also be partially caused by a few unexplained events, where rainfall apparently percolated into the block causing cooling, or possibly by overestimating the effectiveness of the block wall insulation in the model.

Table 5-2. RMSD and MD for Temperature Profile Along TT1 Using Drift-scale Data Set

Time (days)	RMSD (°C)	MD (°C)
30	7.25	6.90
100	14.05	10.55
200	10.56	4.34
300	9.16	1.53
400	5.82	3.53
500	0.63	0.08

The history for TT1-19 (1.76 m below the top of the block) is similar to that observed for TT1-14, except that the agreement with field data is somewhat improved. While the model predicts some superheating between 150 and 235 days, the field temperatures approach but never exceed boiling.

Figure 5-35 shows the comparison of the calculated temperature profiles along TT1, using the DS and the MS property sets, with the measured data. The MS property set overpredicts the temperature at the heater zone more than the DS property set. The degree of agreement with field temperatures between simulation results using the two property sets is examined by comparing the RMSD and MD for profiles along TT1 at various times from 30 days through 500 days. Histories of the RMSD and MD for the two property sets are tabulated in Table 5-3. As shown earlier in the temperature profiles, the DS data set consistently gives a lower RMSD than the MS data set. For both data sets, the match with field data is good at 30 days, worsens at 100 days, and then steadily improves thereafter. The MD is also generally smaller for the DS data set, suggesting better agreement with field data. Again, the accuracy of both predictions consistently increases with time, with a MD of less than 1°C at 500 days, 125 days into the cool-down phase. The TH modeling, as presented in Section 6.2.2.6, will shed some light on the temperature characteristics as shown in Figure 5-35.

Table 5-3. RMSD and MD for Temperature Profile Along TT1 Using Drift-scale and Mountain-scale Property Sets

Time (days)	Drift-scale data		Mountain-scale data	
	RMSD (°C)	MD (°C)	RMSD (°C)	MD (°C)
30	7.25	6.90	7.37	7.02
100	14.05	10.55	15.23	11.11
200	10.56	4.34	12.60	6.05
300	9.16	1.53	10.42	3.38
400	5.82	3.53	6.42	4.27
500	0.63	0.08	0.55	-0.06

5.6.4 Summary

Results of this comparative analysis to assess the performance of the model using the DS and MS data sets are summarized as follows:

- In general, the temperatures predicted by both property sets agree well with the measured data.
- Simulation results obtained using the DS data set show better agreement with the field temperatures than simulation results obtained using the MS data set.
- Both data sets generally overpredict temperature in and adjacent to the heater horizon, but the degree of overprediction is less for the DS data.
- The RMSD and MD for both data sets indicate that the agreement with field data generally increases as the test progresses.
- As mentioned earlier, the LBT was not designed to test rock properties, due to its size and the near-surface setting. Therefore, the conclusion inferred from these comparisons with property sets should be considered as for reference only.

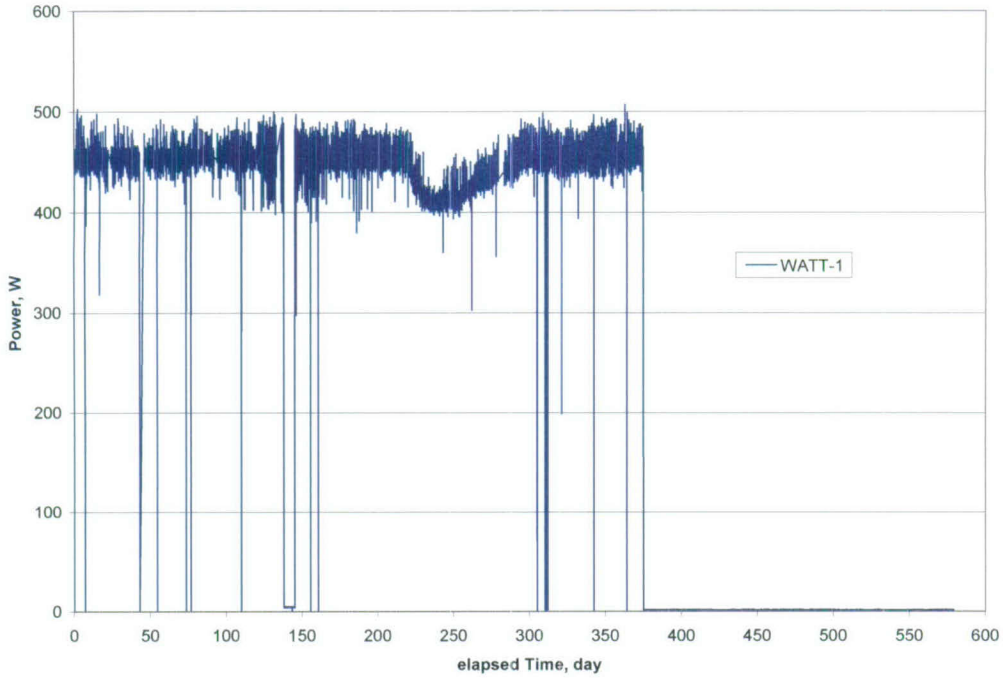

Figure 5-1. The Power Output of the Heater in EH1 as a Function of Time

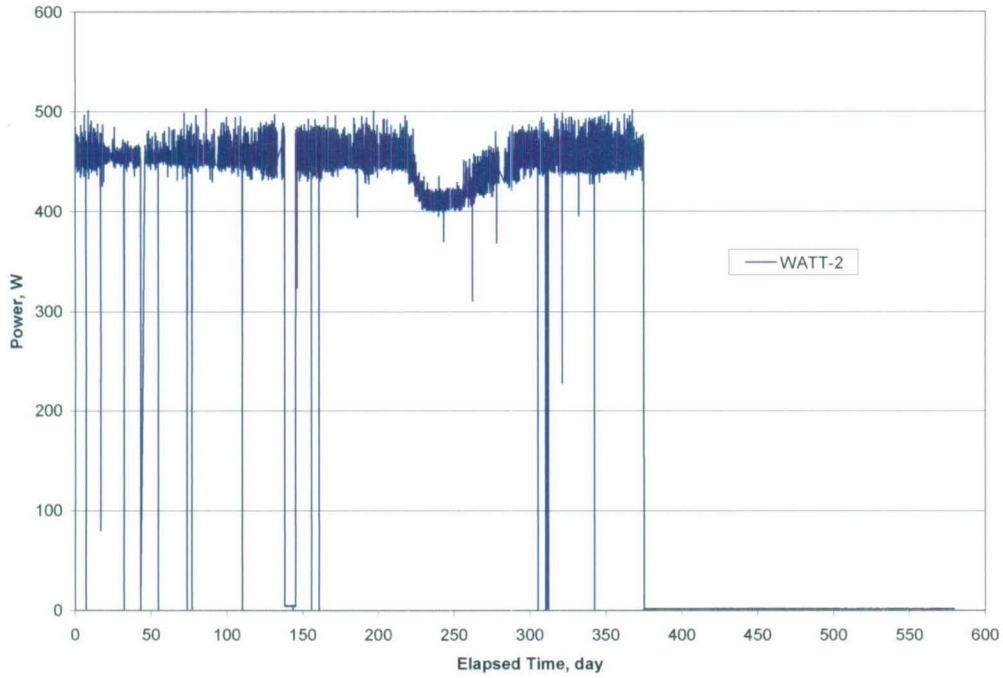

Figure 5-2. The Power Output of the Heater in EH2 as a Function of Time

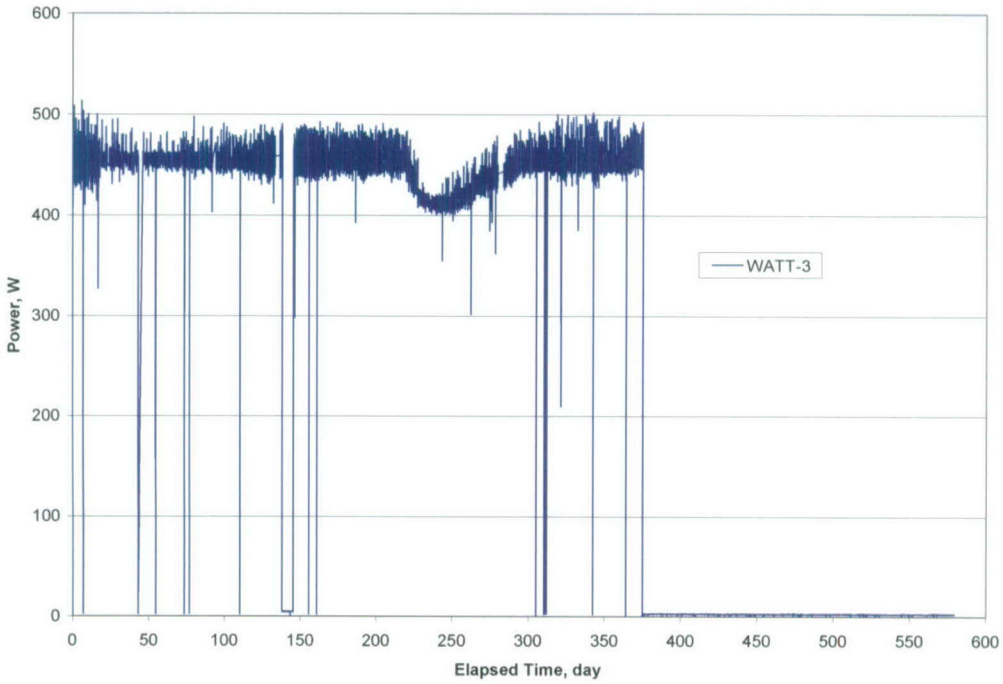

Figure 5-3. The Power Output of the Heater in EH3 as a Function of Time

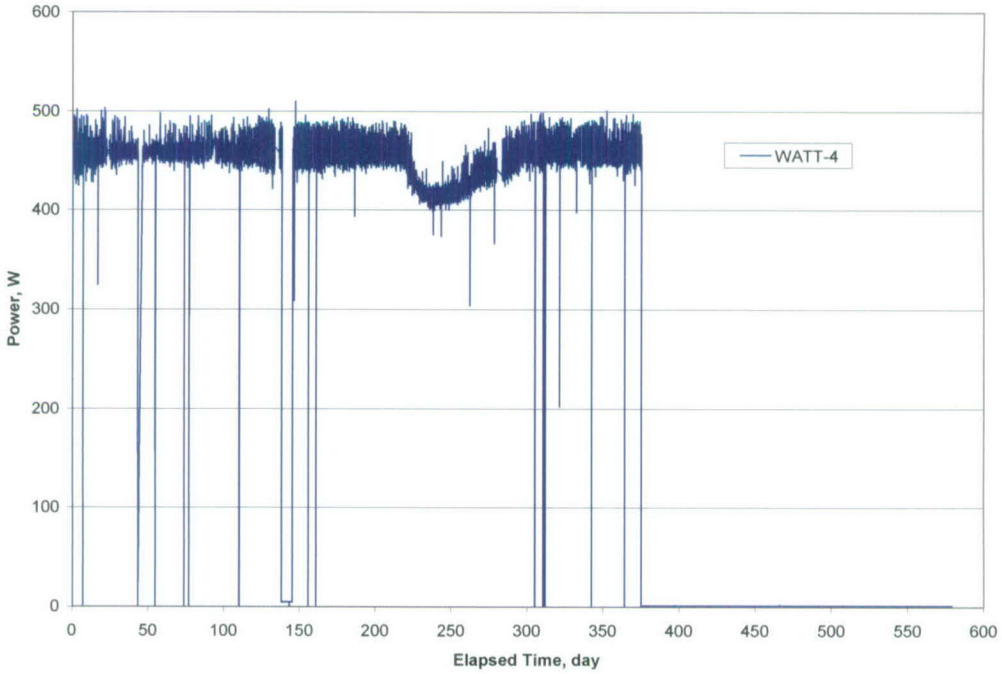

Figure 5-4. The Power Output of the Heater in EH4 as a Function of Time

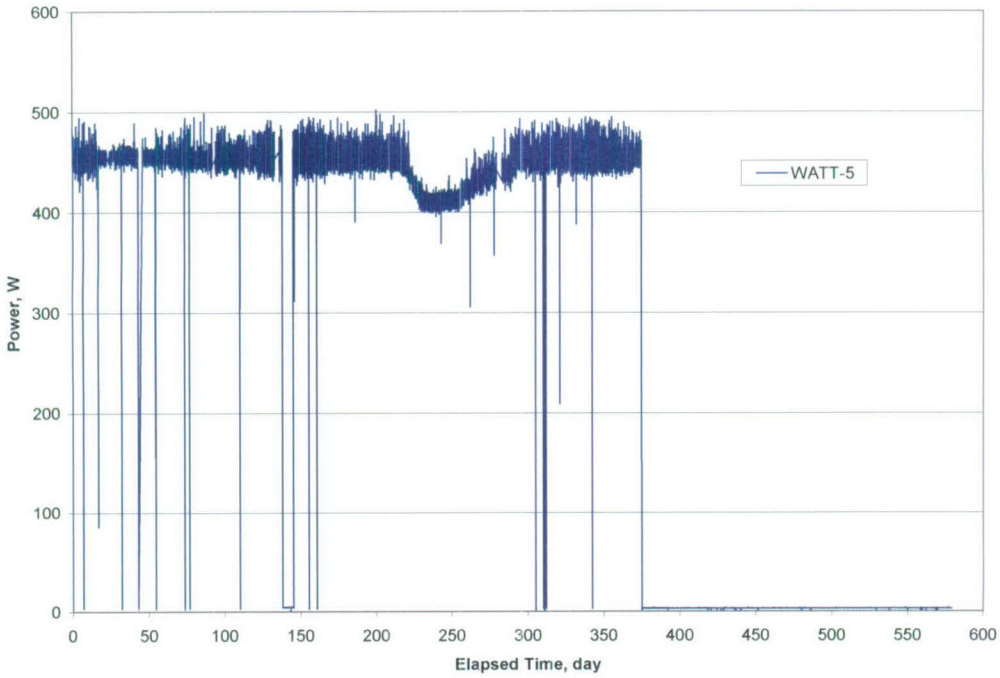

Figure 5-5. The Power Output of the Heater in EH5 as a Function of Time

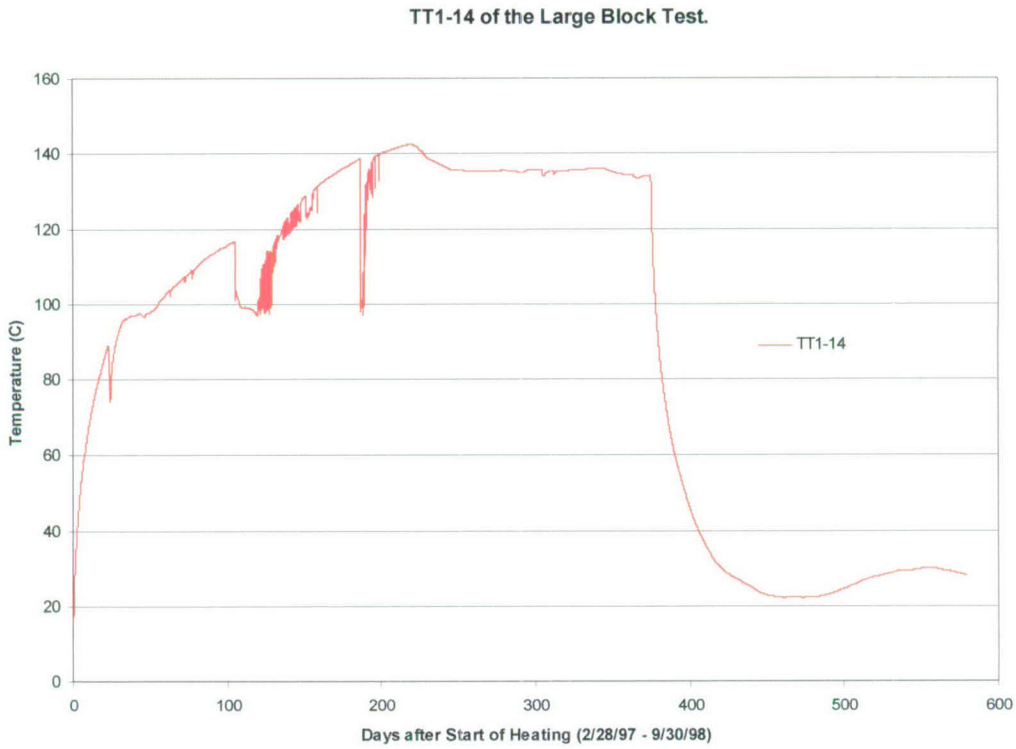

Figure 5-6. Temperature at TT1-14 as a Function of Time

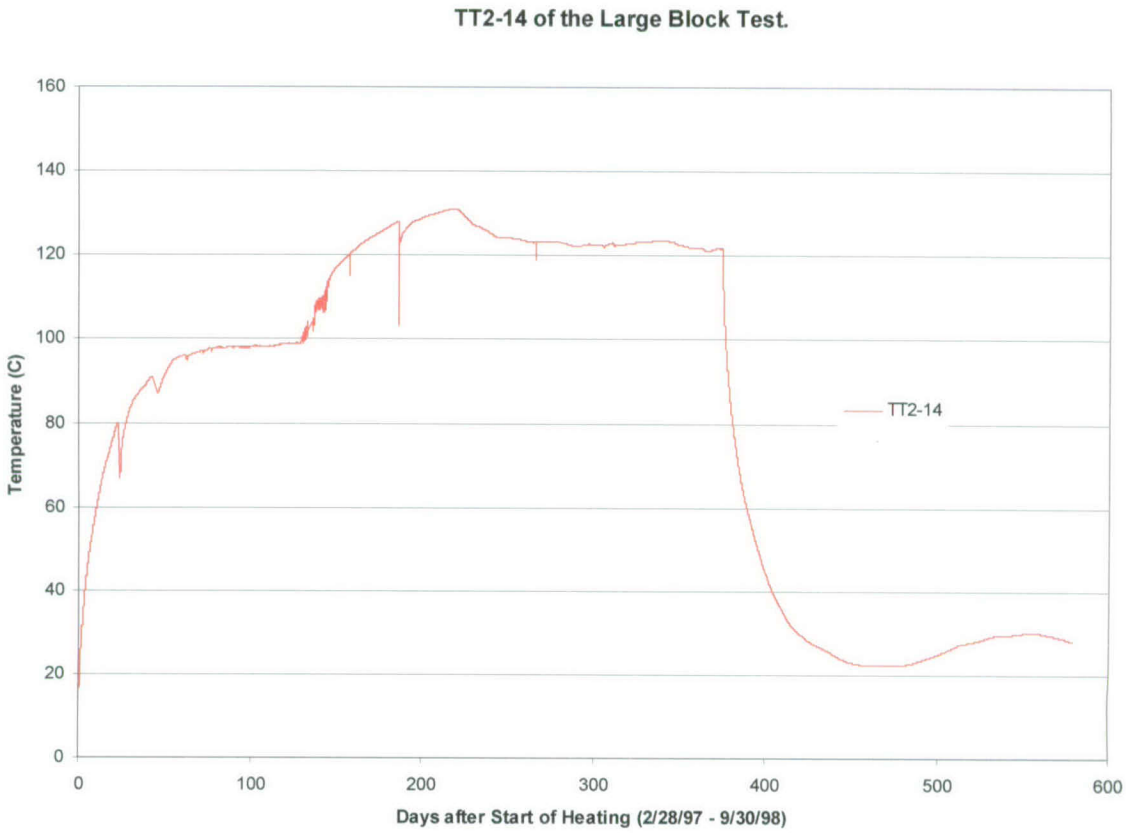

Figure 5-7. Temperature at TT2-14 as a Function of Time

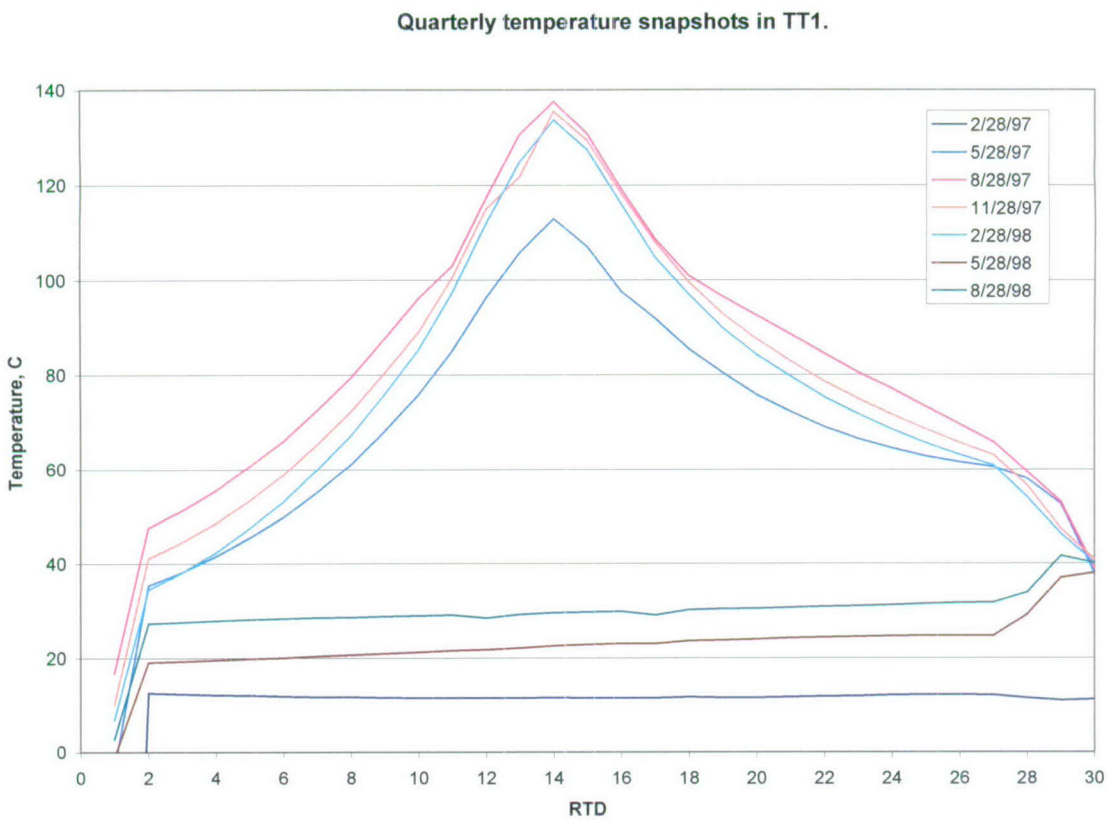

NOTE: RTD 1 is at the bottom of the hole.

Figure 5-8. Quarterly Temperature Snapshots in TT1 to Show the Spatial Temperature Variation

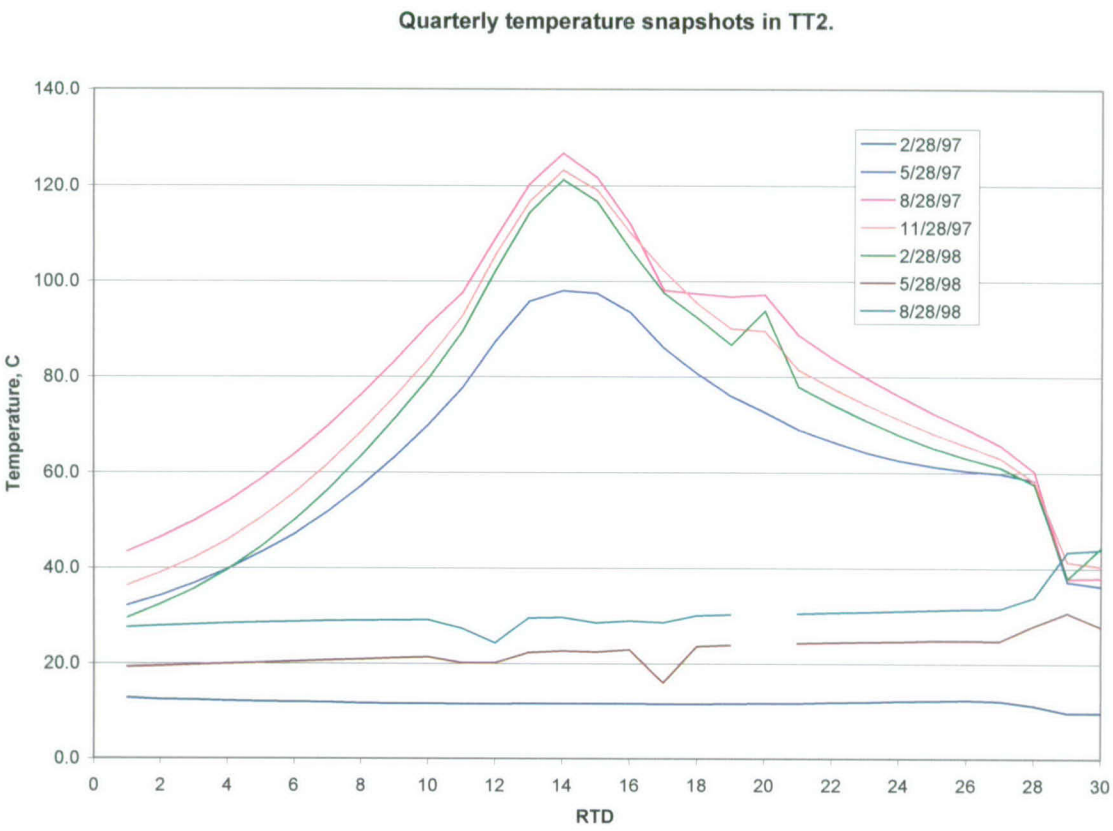

NOTE: RTD 1 is at the bottom of the hole.

Figure 5-9. Quarterly Temperature Snapshots in TT2 to Show the Spatial Temperature Variation

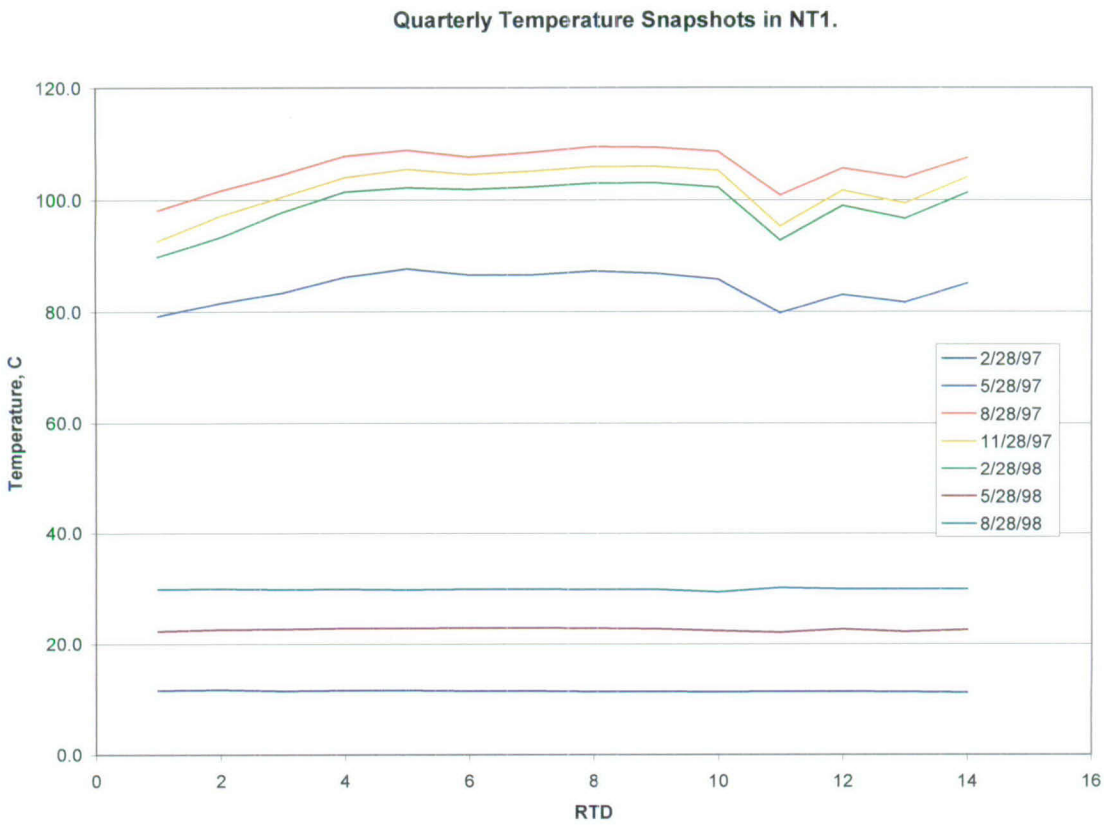

NOTE: RTD 1 is near the north face; RTD 14 is near the south face.

Figure 5-10. Quarterly Temperature Snapshots in NT1 to Show the Spatial Temperature Variation

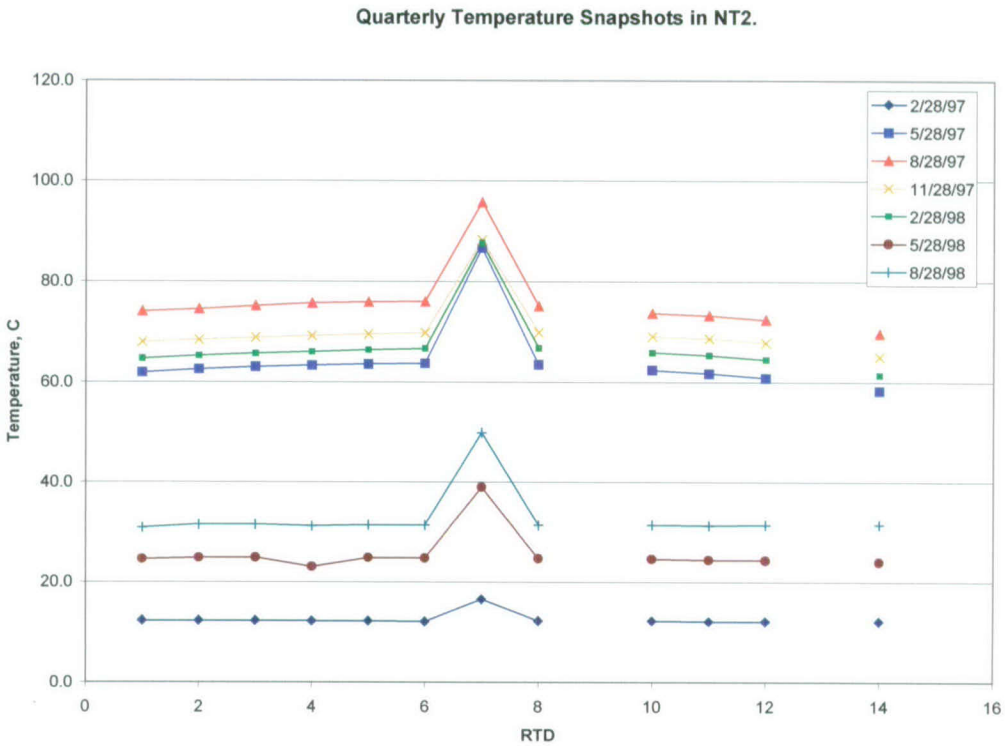

NOTE: RTD 1 is near the north face; RTD 14 is near the south face.

Figure 5-11. Quarterly Temperature Snapshots in NT2

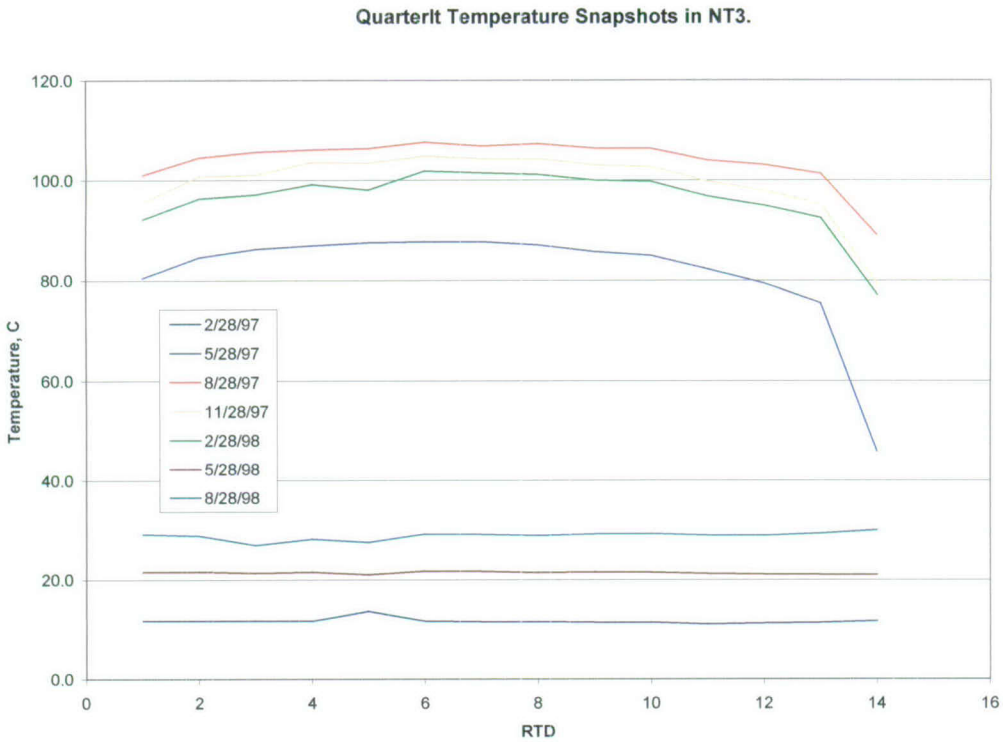

NOTE: RTD1 is near the north face; RTD 14 is near the south face.

Figure 5-12. Quarterly Temperature Snapshots in NT3 to Show the Spatial Temperature Variation

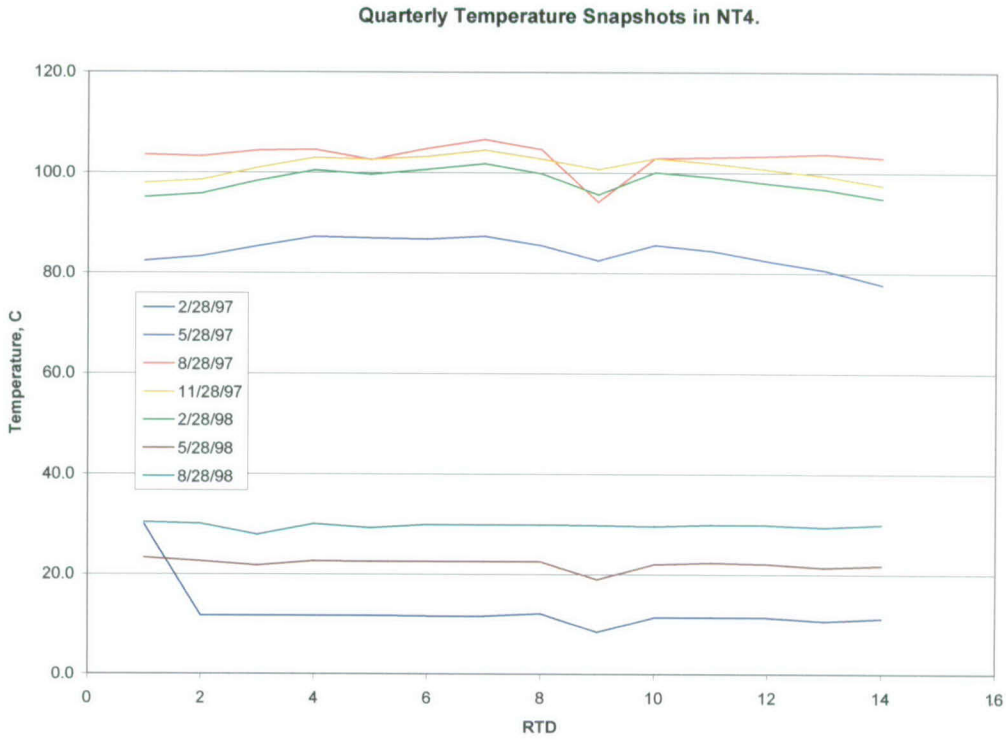

NOTE: RTD 1 is near the north face; RTD 14 is near the south face.

Figure 5-13. Quarterly Temperature Snapshots in NT4 to Show the Spatial Temperature Variation

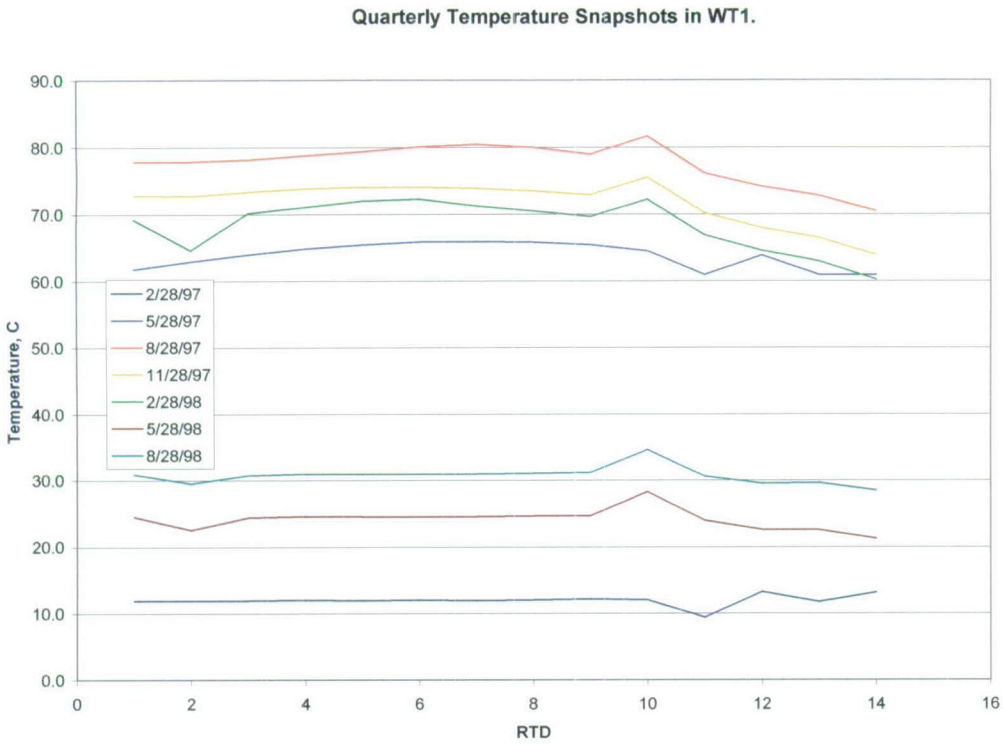

NOTE: RTD1 is near the west face; RTD 14 is near the east face.

Figure 5-14. Quarterly Temperature Snapshots in WT1 to Show the Spatial Temperature Variation

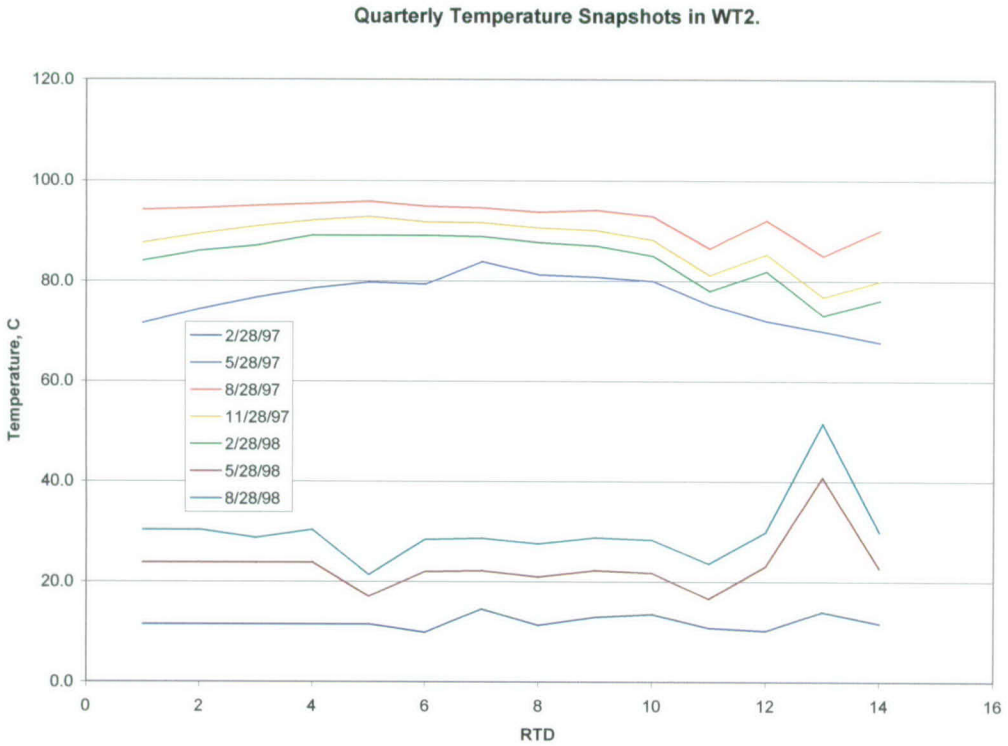

NOTE: RTD1 is near the west face; RTD 14 is near the east face.

Figure 5-15. Quarterly Temperature Snapshots in WT2 to Show the Spatial Temperature Variation

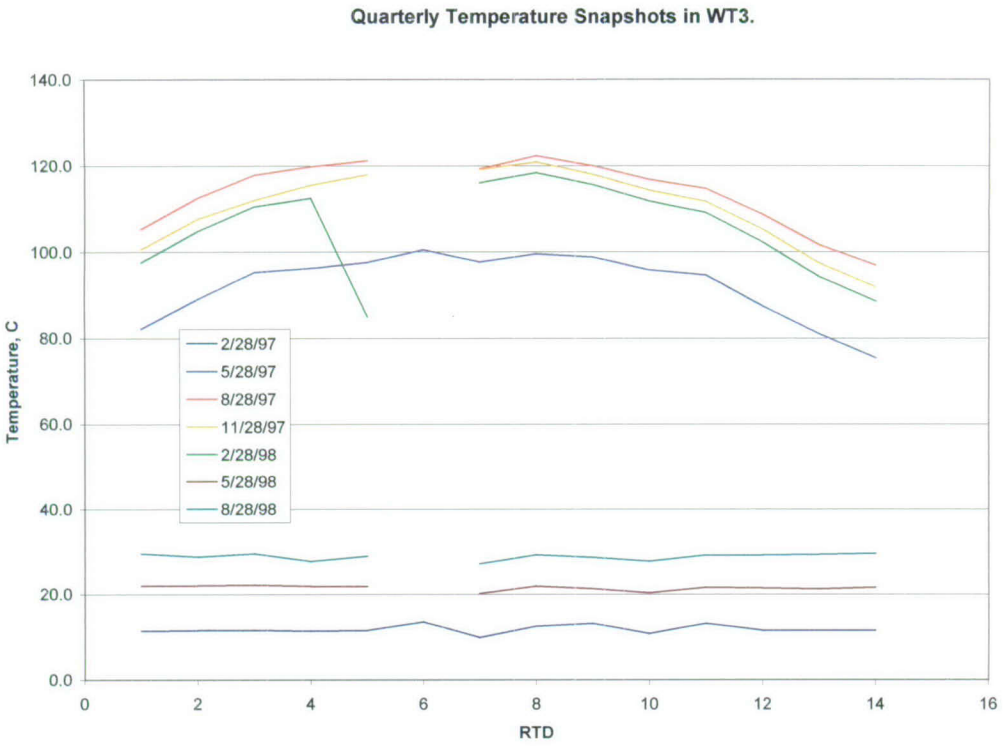

NOTE: RTD1 is near the west face; RTD 14 is near the east face.

Figure 5-16. Quarterly Temperature Snapshots in WT3 to Show the Spatial Temperature Variation

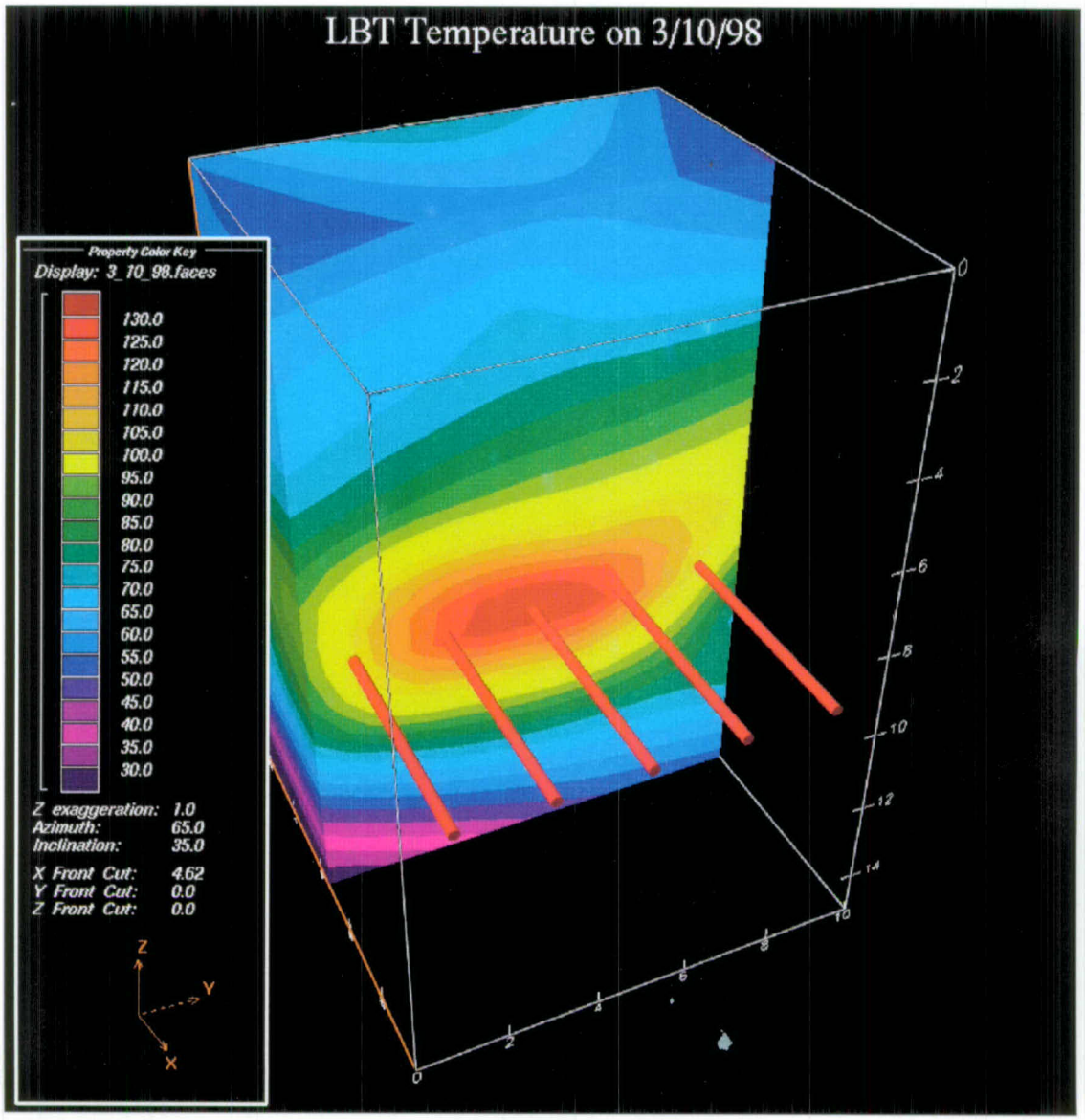

Figure 5-17. The Vertical Cross Section Along TT1 of the 3-D Temperature Field in the Block on March 10, 1998

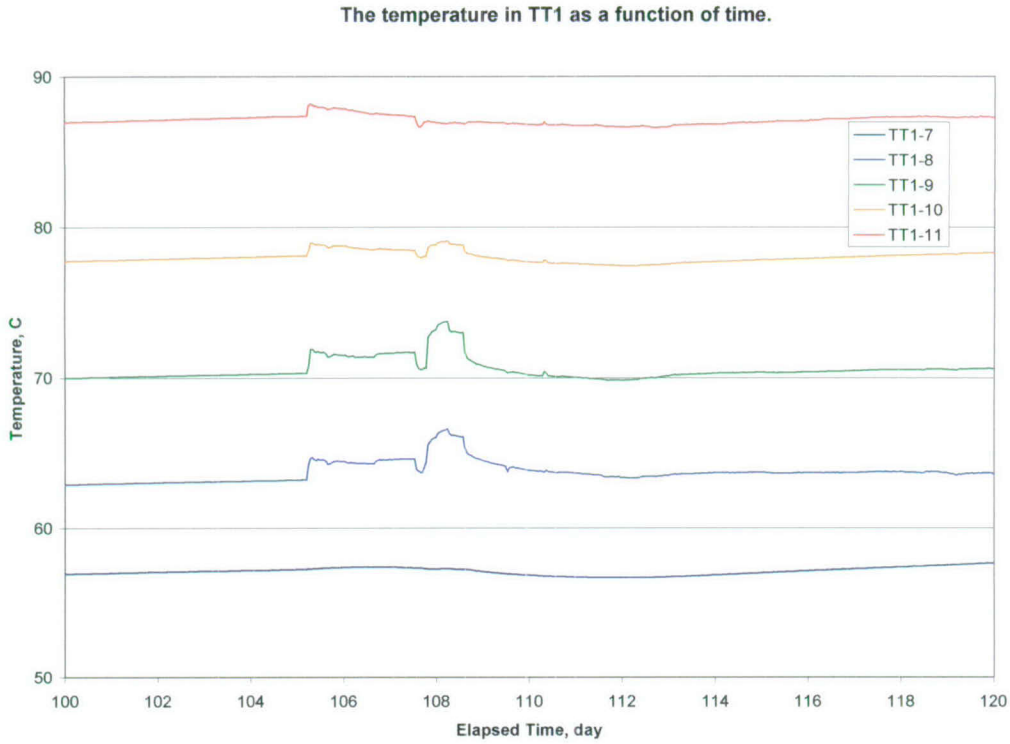

Figure 5-18. The Temperature at TT1-7 to TT1-11, Showing the Effect of the TH event on June 13, 1997 (105.2 Day)

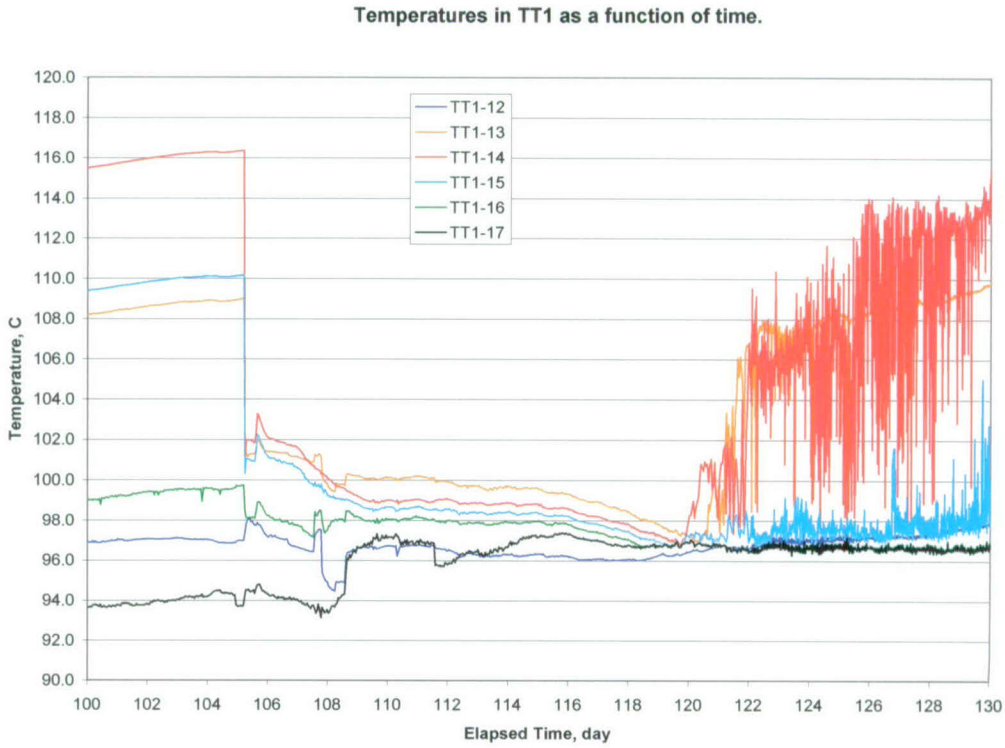

Figure 5-19. The Temperature at TT1-12 to TT1-17, Showing the Effect of the TH Event on June 13, 1997 (105.2 Day)

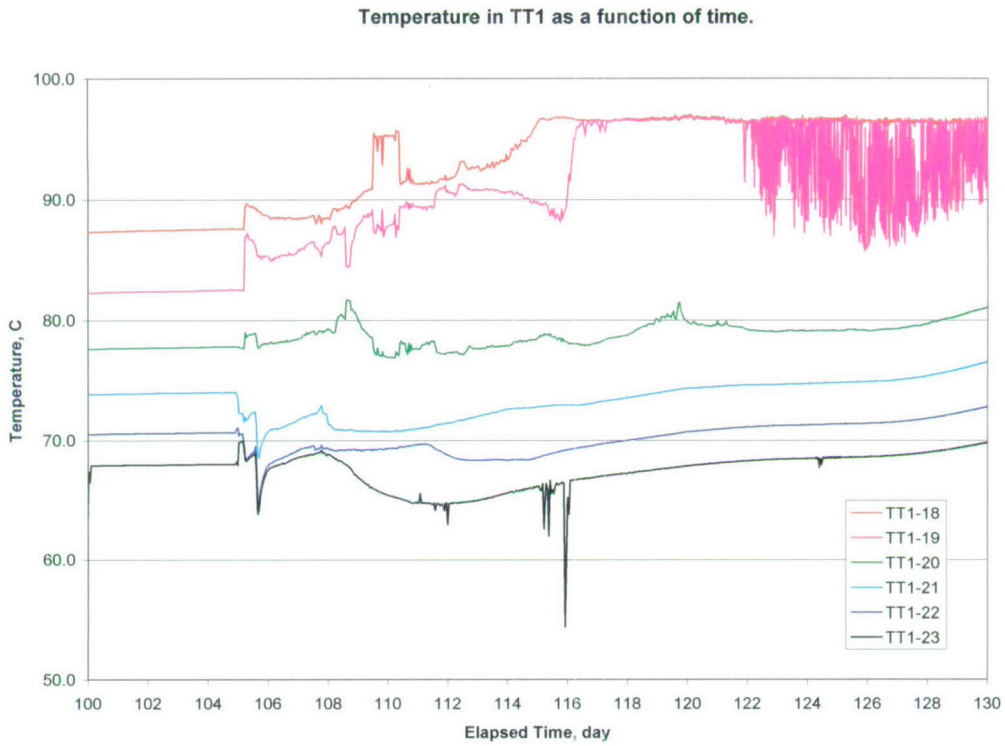

Figure 5-20. The Temperature at TT1-18 to TT1-23, Showing the Effect of the TH Event on June 13, 1997 (105.2 Day)

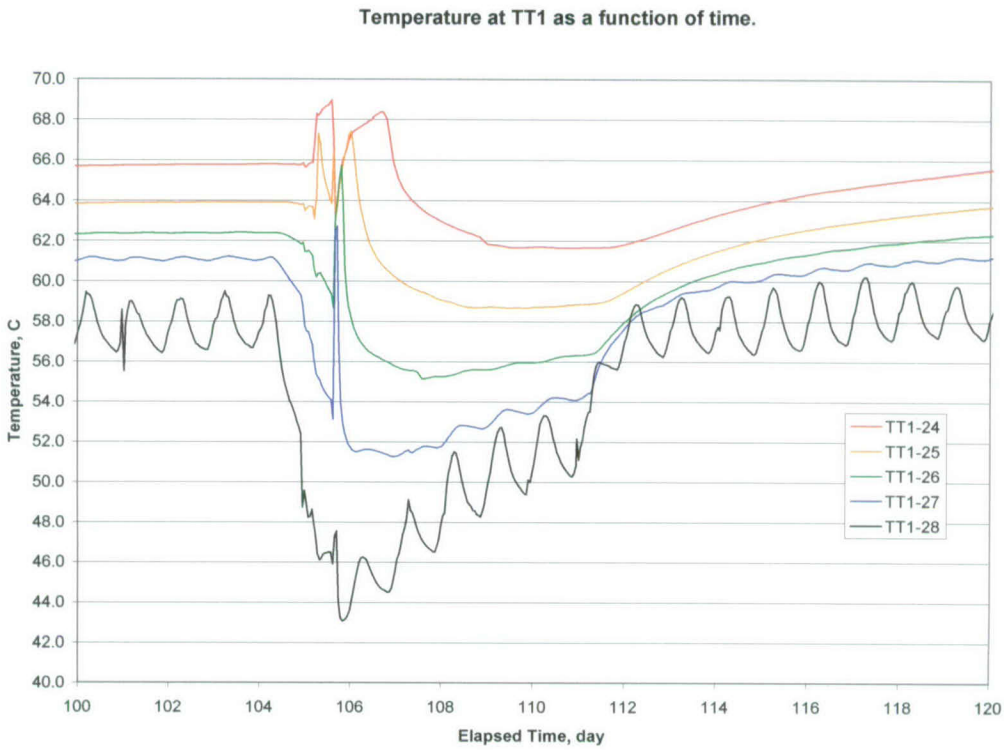

Figure 5-21. Temperature at TT1-24 to TT1-28, Showing the Effect of the TH Event on June 13, 1997 (105.2 Day)

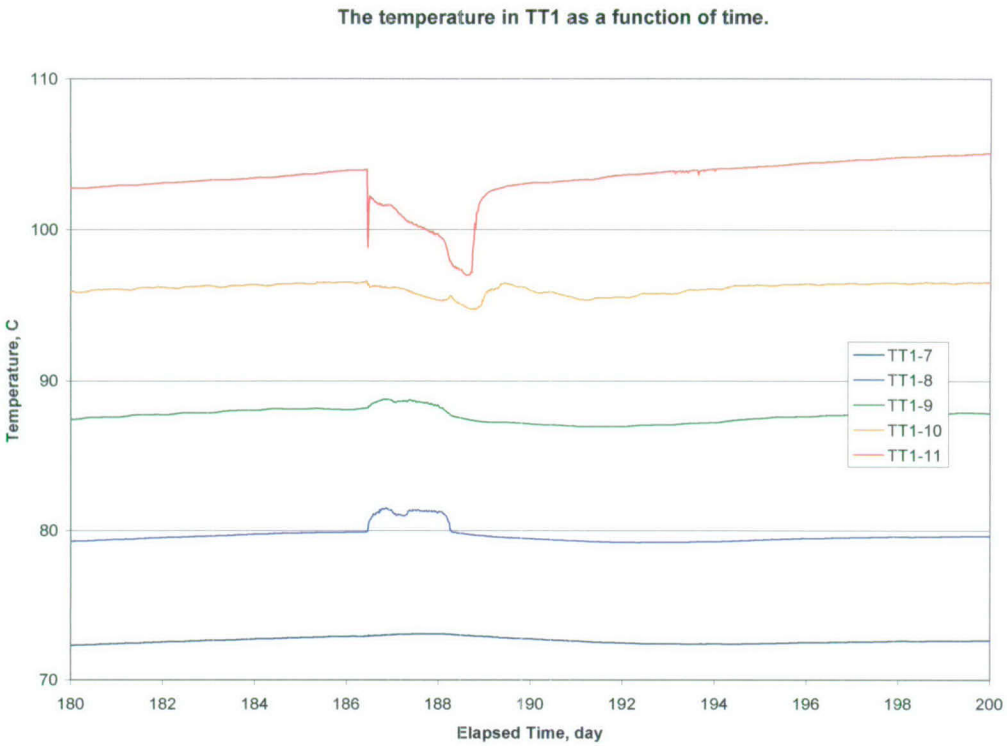

Figure 5-22. The Temperature at TT1-7 to TT1-11 as a Function of Time, Showing the Effect of the TH Event on September 2, 1997 (186.5 Day)

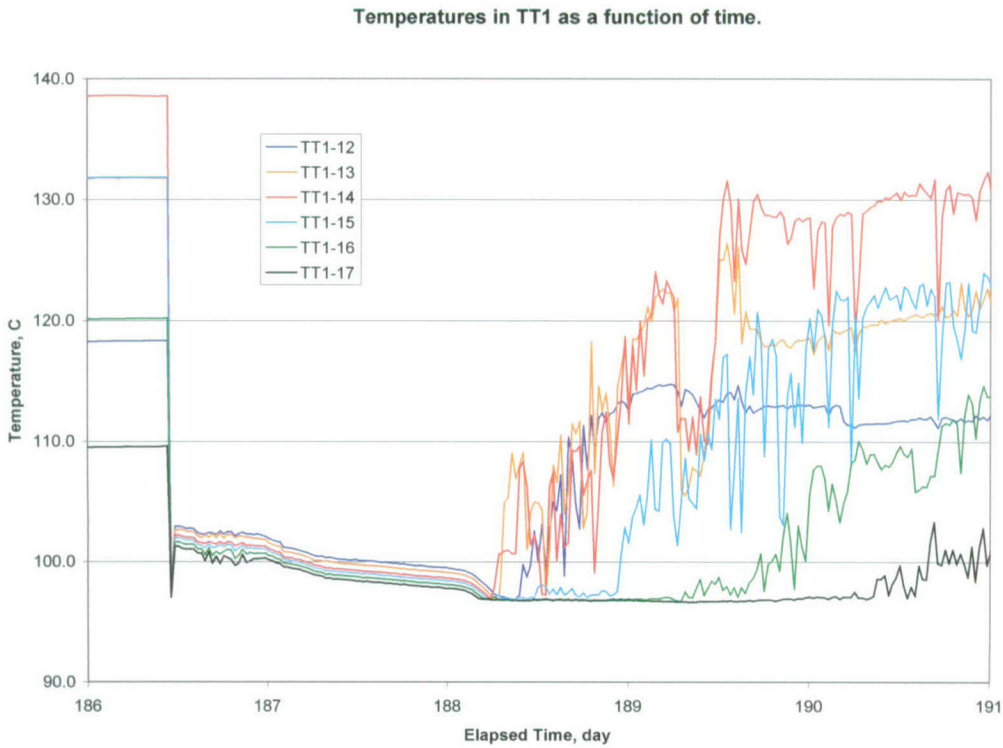

Figure 5-23. The Temperature at TT1-12 to TT1-17 as a Function of Time, Showing the TH Event on September 2, 1997 (186.5 Day)

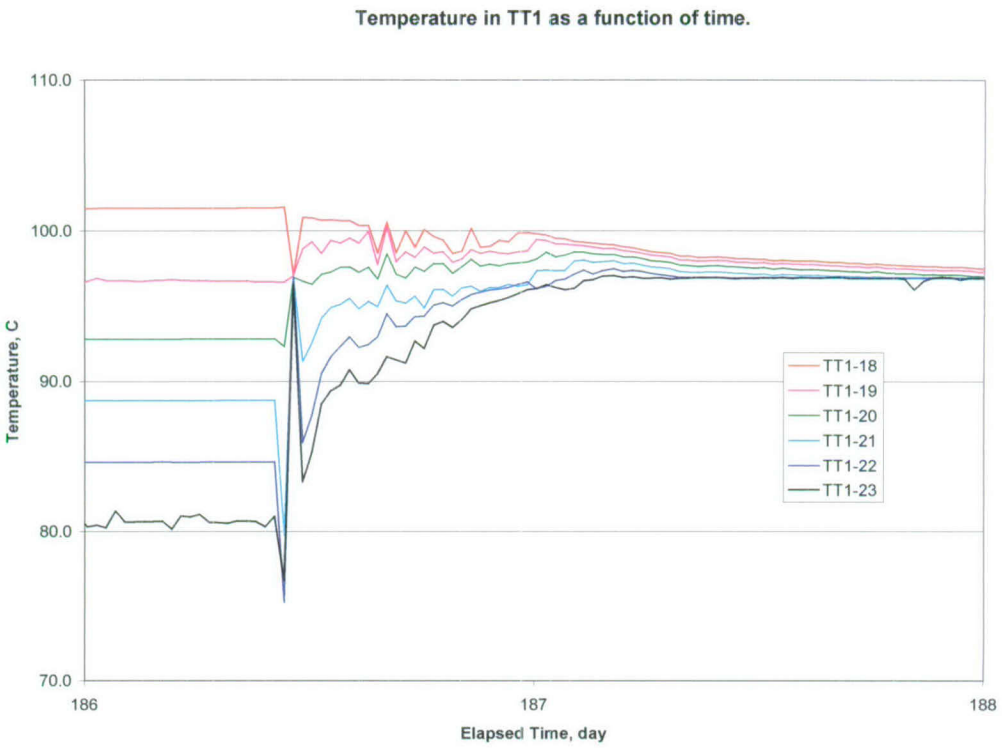

Figure 5-24. The Temperature at TT1-18 to TT1-23, Showing the Effect of the TH Event on September 2, 1997 (186.5 Day)

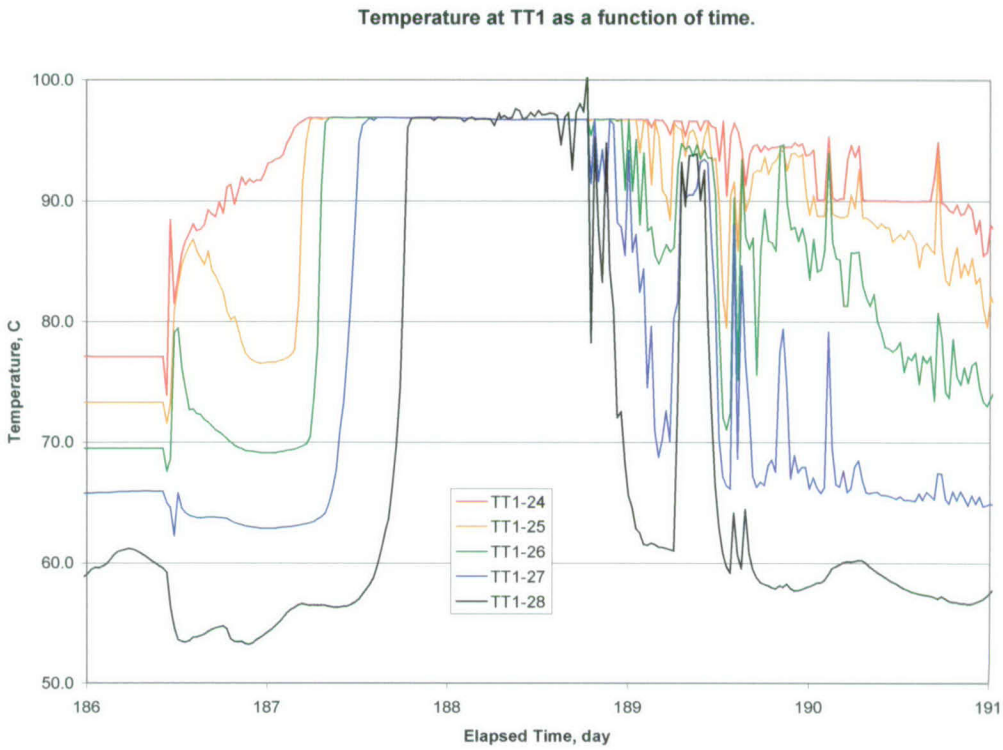

Figure 5-25. The Temperature at TT1-24 to TT1-28, Showing the Effect of the TH event on September 2, 1997 (186.5 Day)

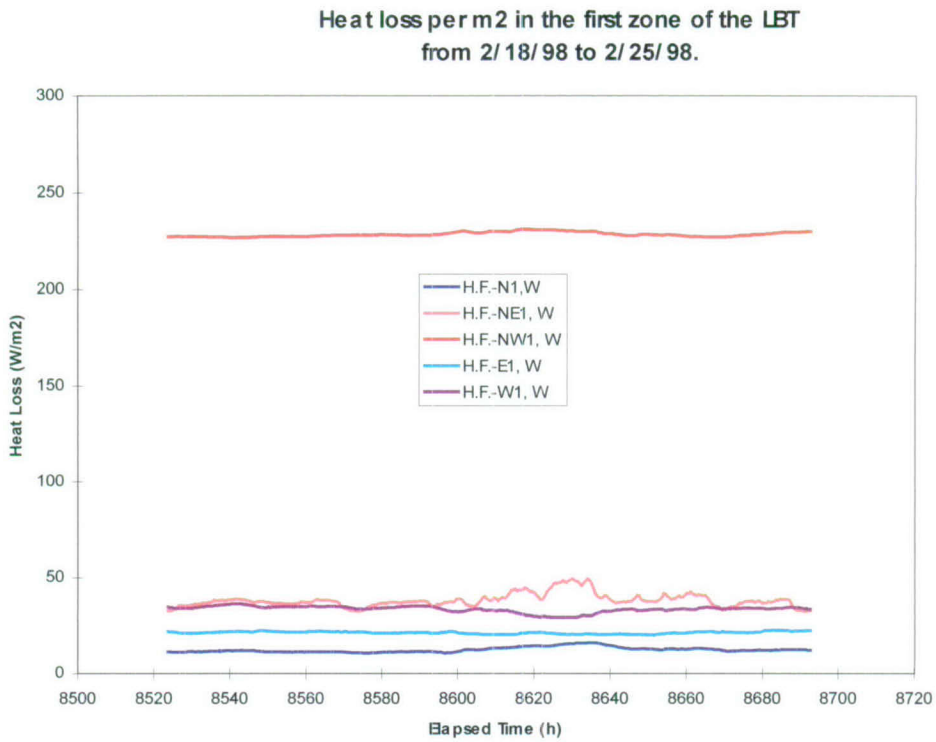

Figure 5-26. The Heat Flux per Unit Area in Zone 1 (z = –3.2 to –4.42 m) of the Block as a Function of Time from February 18, 1998, to February 25, 1998

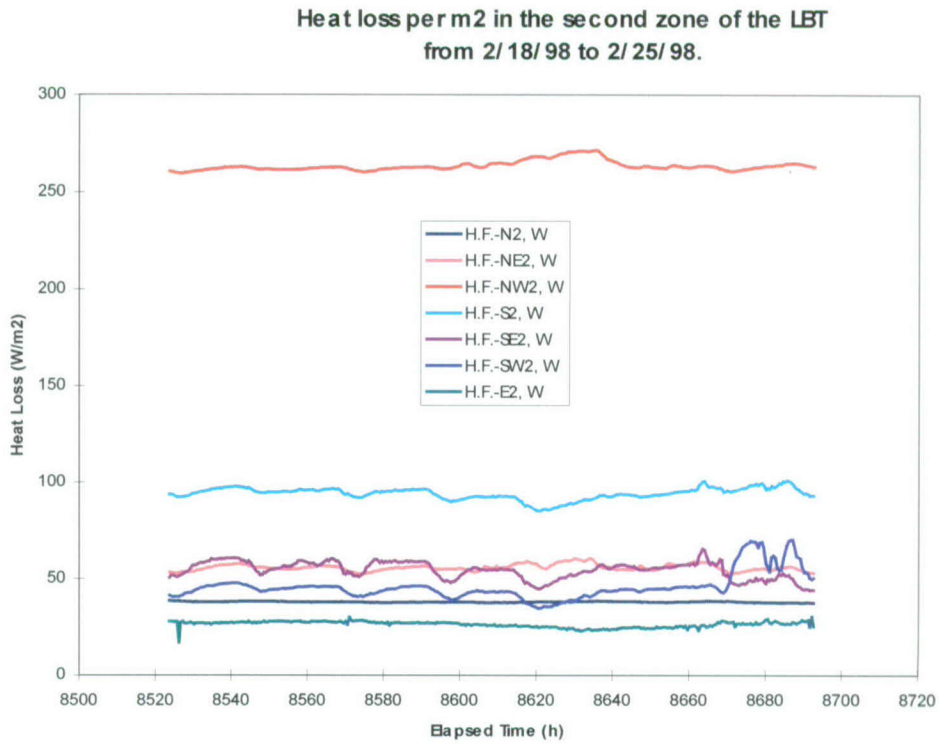

Figure 5-27. The Heat Flux per Unit Area in Zone 2 (z = –1.981 to –3.2 m) of the Block as a Function of Time from February 18, 1998, to February 25, 1998

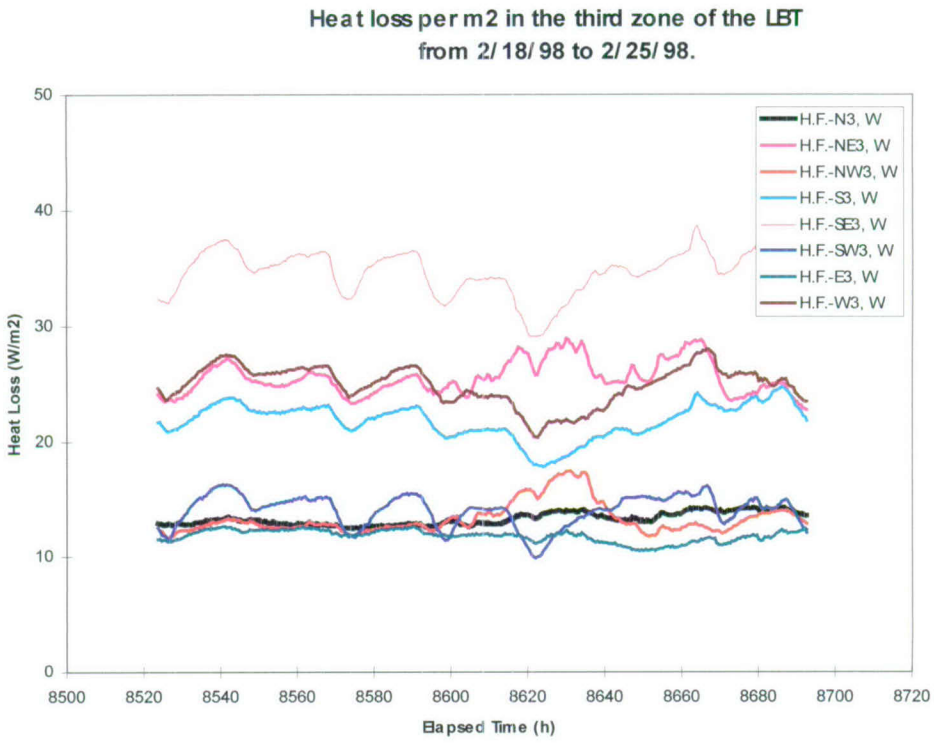

Figure 5-28. The Heat Flux per Unit Area in Zone 3 (z = –0.762 to –1.981 m) of the Block as a Function of Time from February 18, 1998, to February 25, 1998

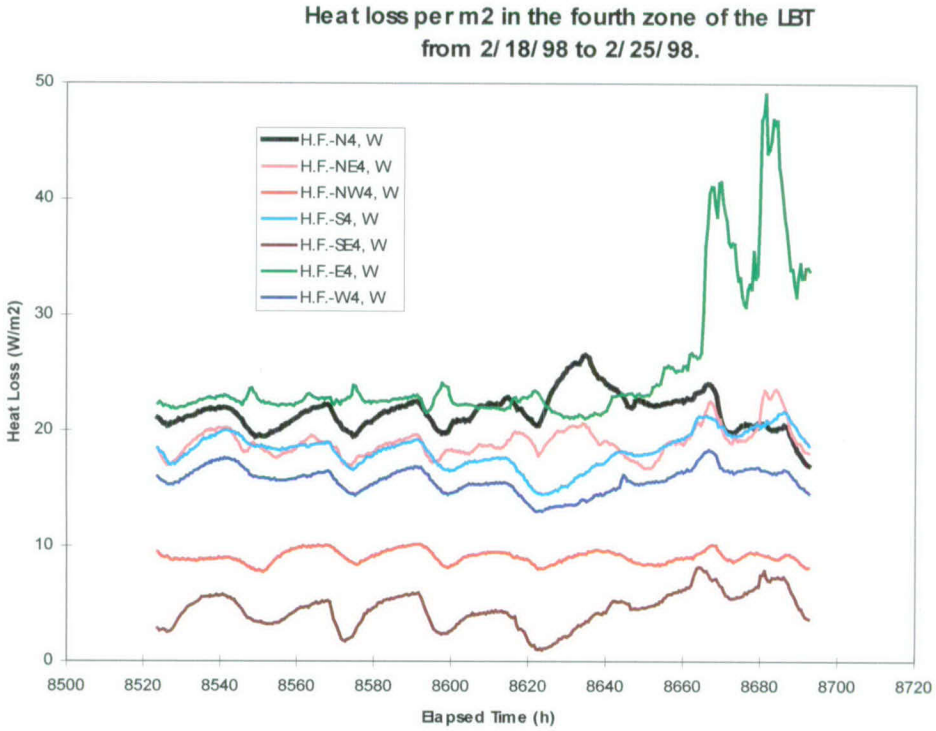

Figure 5-29. The Heat Flux per Unit Area in Zone 4 (z = 0 to –0.762 m) of the Block as a Function of Time from February 18, 1998, to February 25, 1998

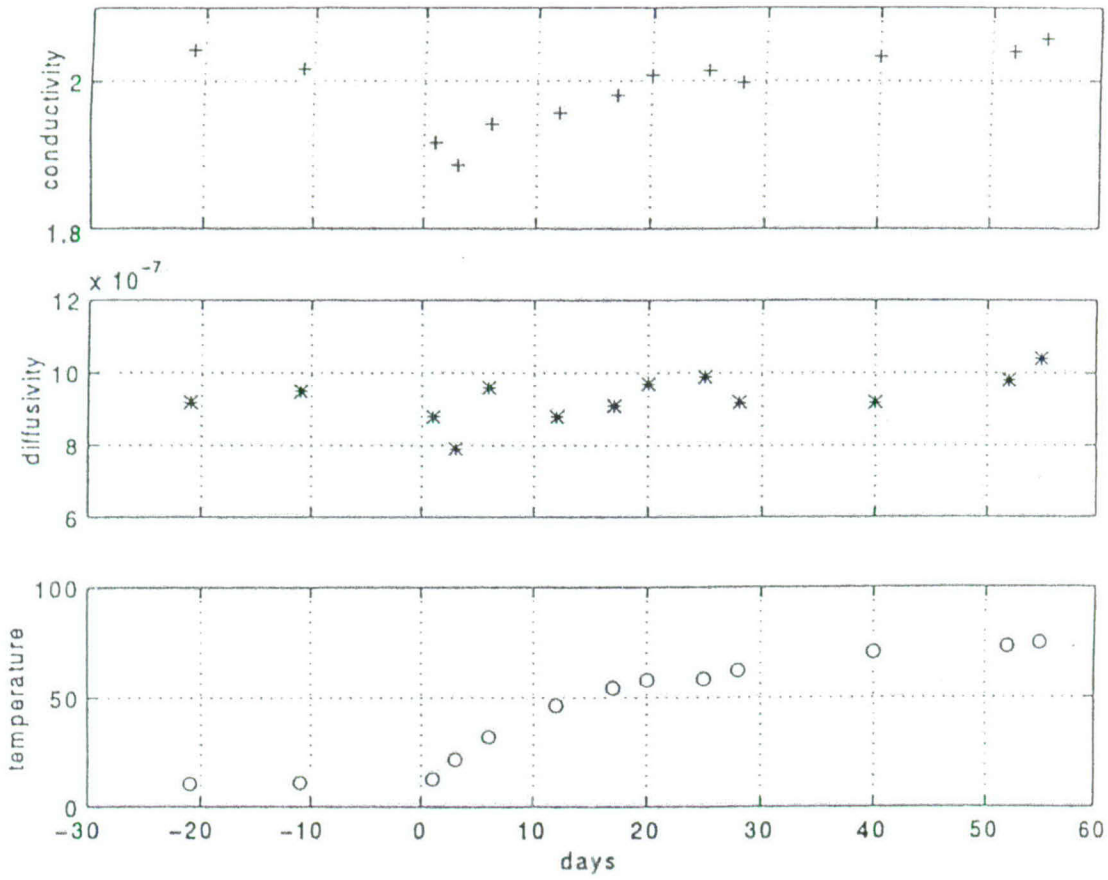

Figure 5-30. Rock Thermal Conductivity, K [W/(mK)], Diffusivity, Alpha [m^2/s], and Temperature [^oC] with Time [Days] for the Horizontal REKA Probe 1 Installed 0.584 m Below the Large Block's Horizontal Heater Layer

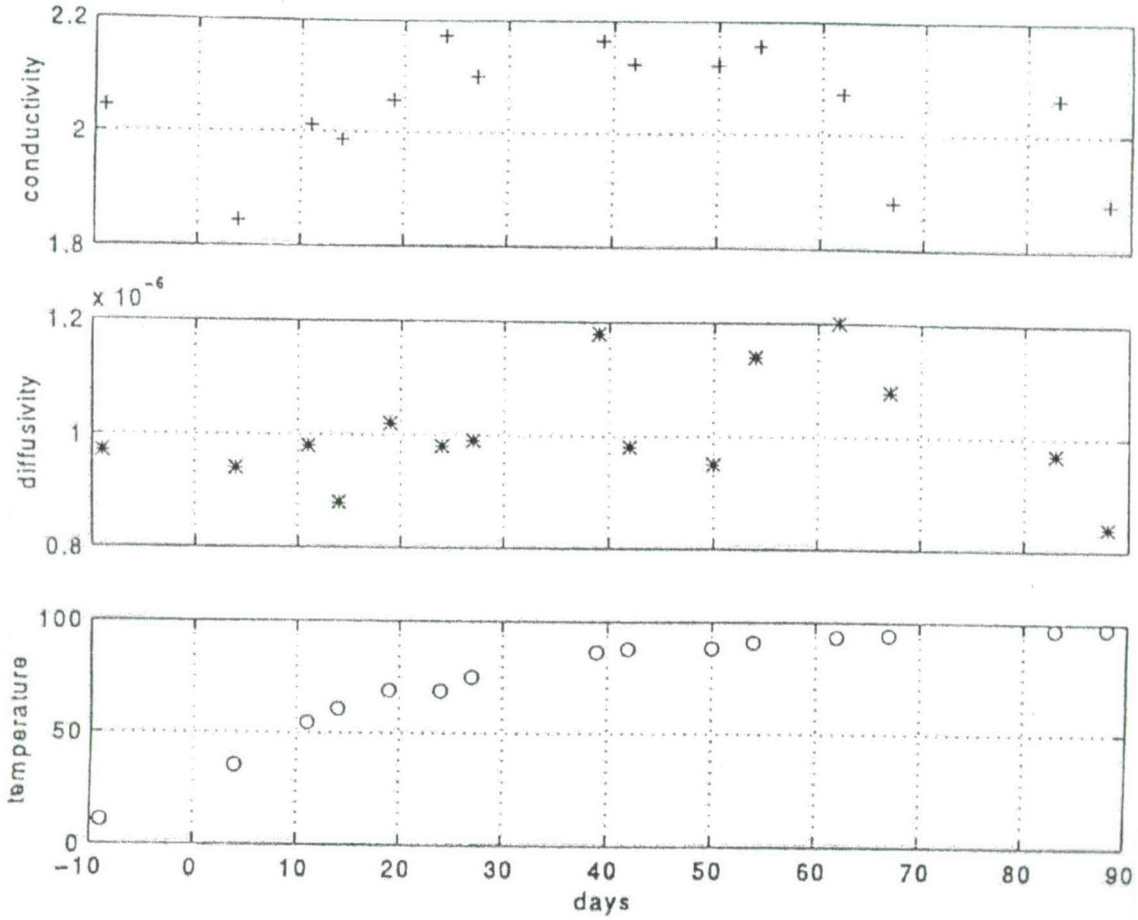

Figure 5-31. Rock Thermal Conductivity, K [W/(mK)], Diffusivity, Alpha [m^2/s], and Temperature [^oC] with Time [Days] for the Horizontal REKA Probe 2 Installed 0.889 m Below the Large Block's Horizontal Heater Layer

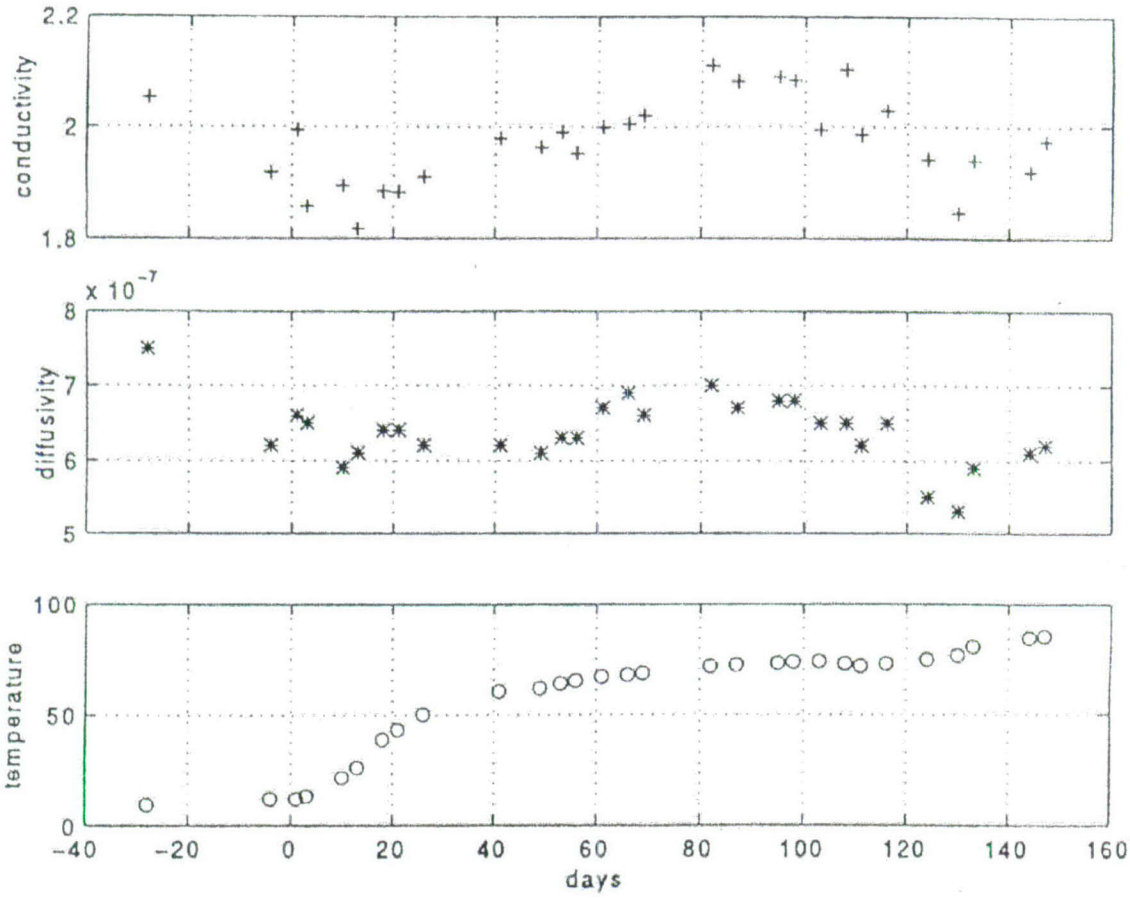

Figure 5-32. Rock Thermal Conductivity, K [W/(mK)], Diffusivity, Alpha [m^2/s], and Temperature [°C] with Time [Days] for the Horizontal REKA Probe 3 Installed 1.38 m Below the Large Block's Horizontal Heater Layer

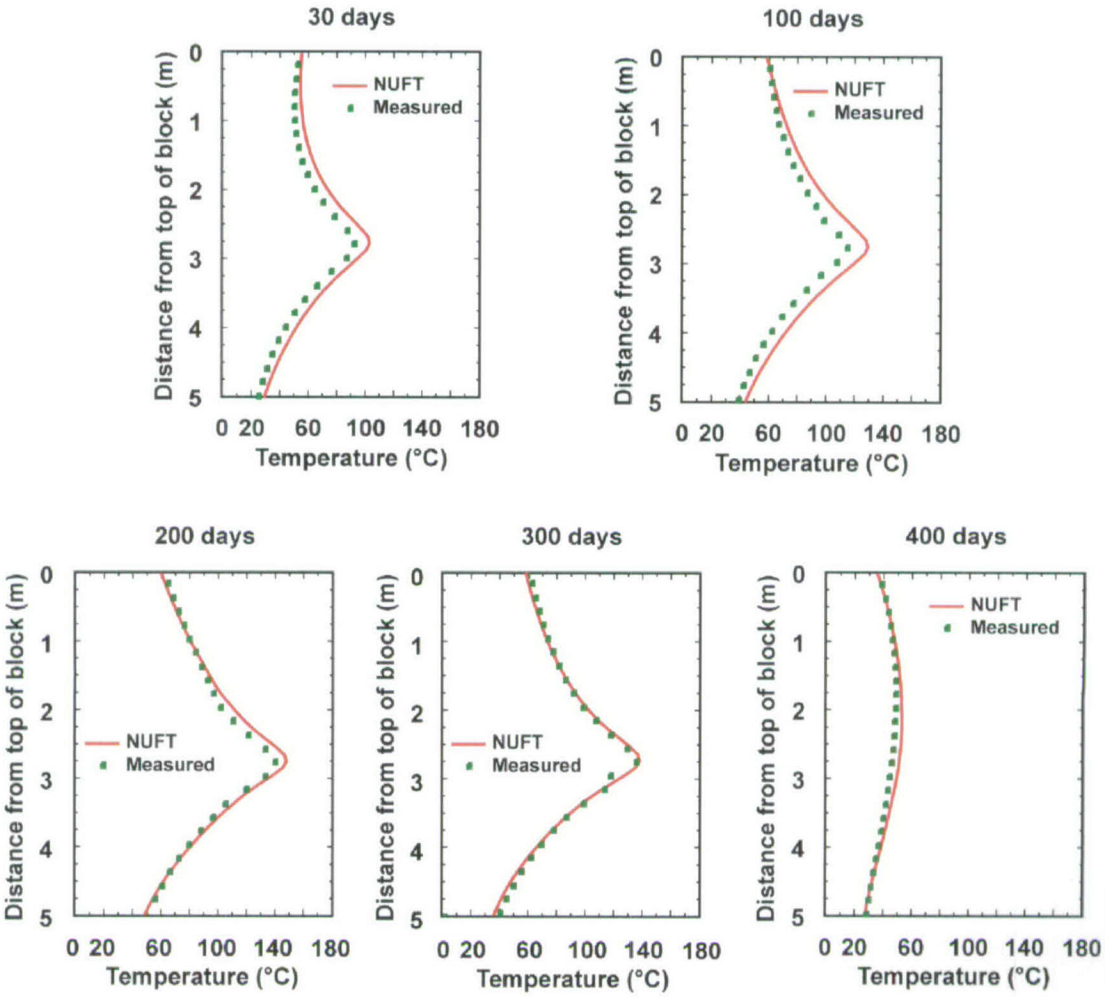

Figure 5-33. The Measured Temperatures in the LBT in TT1 Compared with Model Calculation Using NUFT

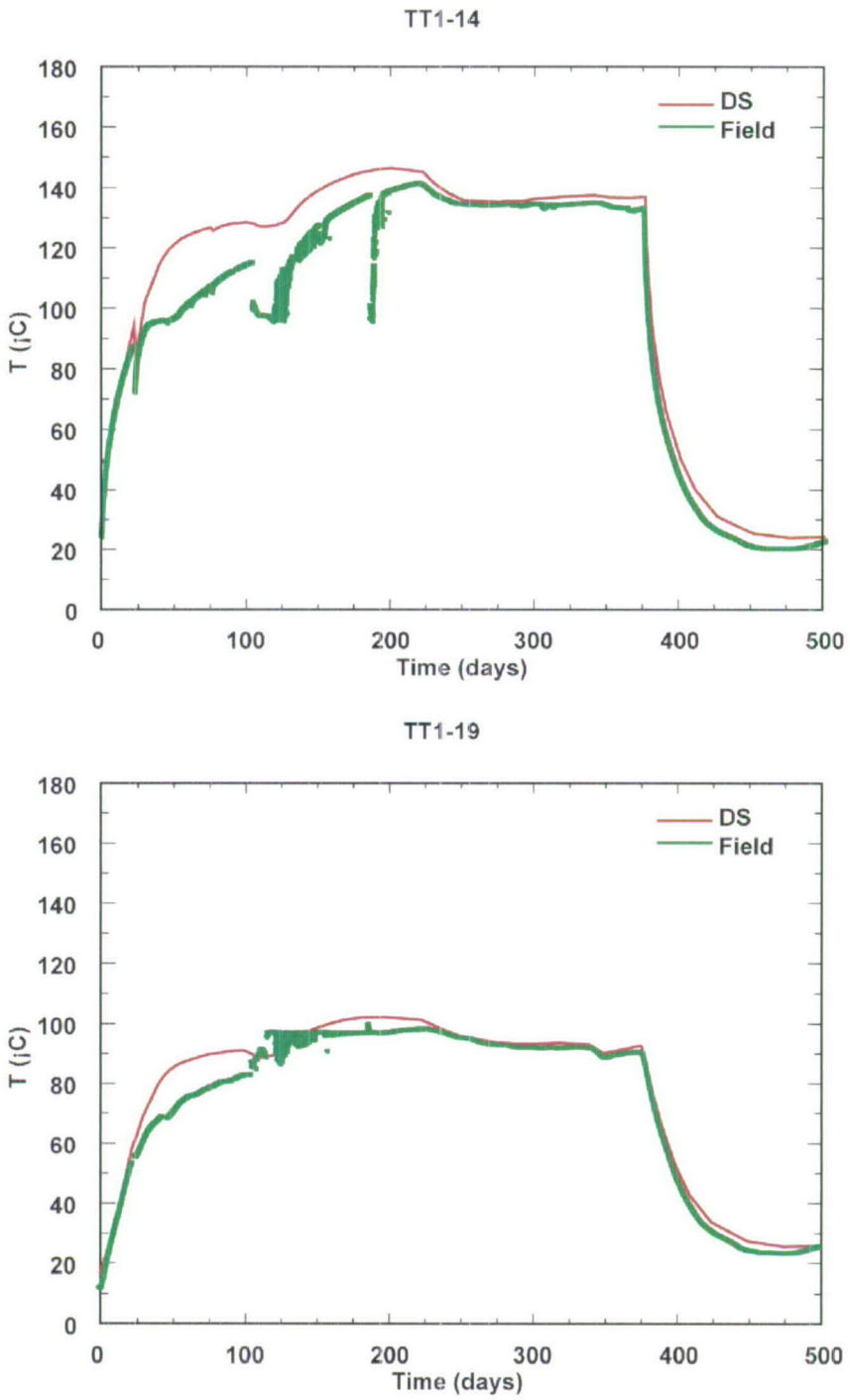

Figure 5-34. Comparison of the Measured Temperature at TT1-14 and TT1-19 with the Model Calculation Using the Drift-Scale Property Set

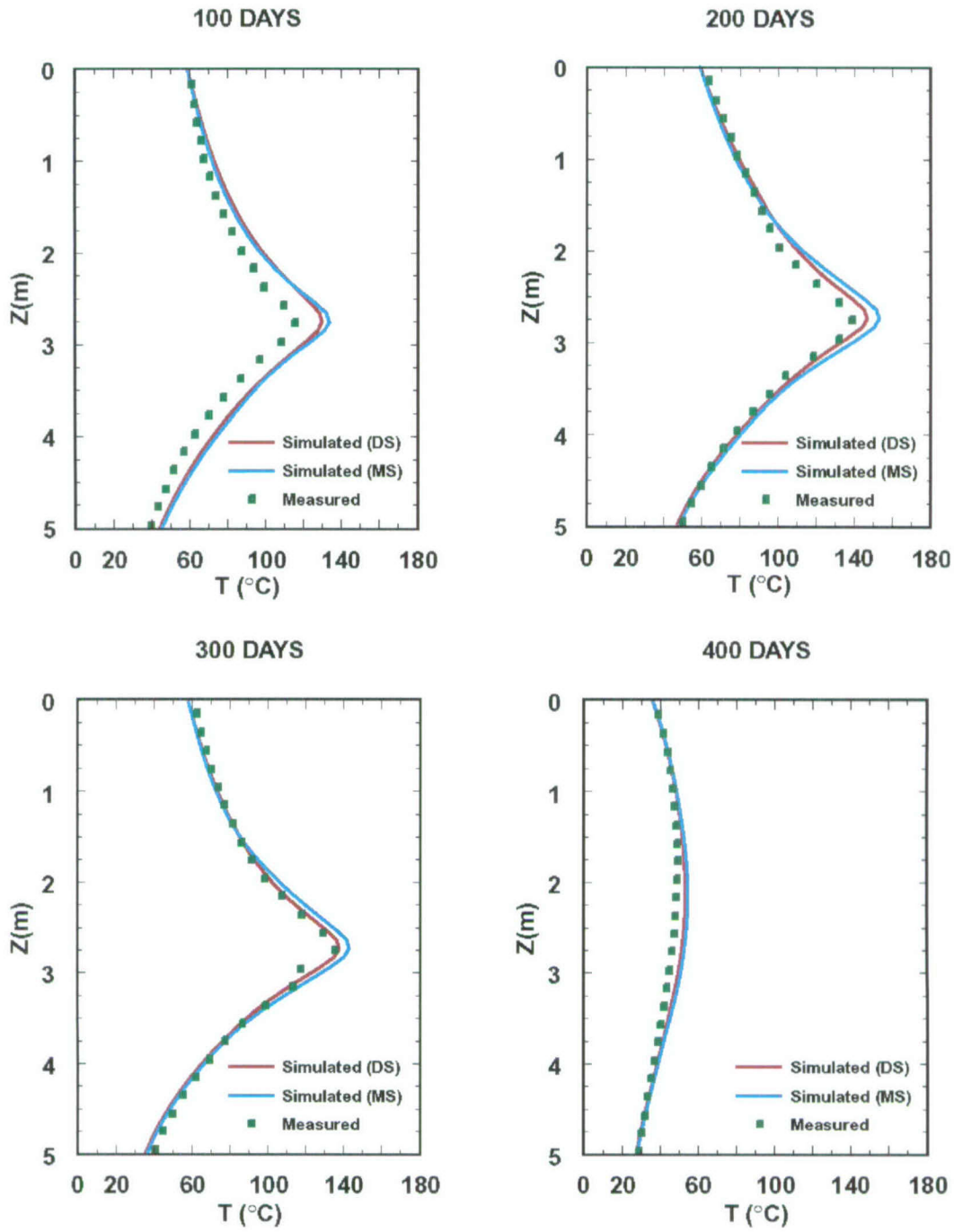

Figure 5-35. Predicted Temperature Profiles Along Hole #TT1 of the LBT Using the DS and MS Property Sets, Compared with the Measured Temperature